Novel amino-functionalized lignin microspheres: High performance biosorbent with enhanced capacity for heavy metal ion removal

Ana L. Popovic, Jelena D. Rusmirovic, Zlate Velickovic, Zeljko Radovanovic, Mirjana Ristic, Vera P. Pavlovic, Aleksandar D. Marinkovic

PII: S0141-8130(19)37149-1

DOI: https://doi.org/10.1016/j.ijbiomac.2019.11.152

Reference: BIOMAC 13933

To appear in: *International Journal of Biological Macromolecules*

Received date: 5 September 2019

Revised date: 13 November 2019

Accepted date: 18 November 2019

Please cite this article as: A.L. Popovic, J.D. Rusmirovic, Z. Velickovic, et al., Novel amino-functionalized lignin microspheres: High performance biosorbent with enhanced capacity for heavy metal ion removal, *International Journal of Biological Macromolecules*(2019), https://doi.org/10.1016/j.ijbiomac.2019.11.152

Novel amino-functionalized lignin microspheres: high performance biosorbent with enhanced capacity for heavy metal ion removal

Ana L. Popovic[a], *Jelena D. Rusmirovic*[b,c*], *Zlate Velickovic*[d], *Zeljko Radovanovic*[c], *Mirjana Ristic*[a], *Vera P. Pavlovic*[e], *Aleksandar D. Marinkovic*[a]

[a]University of Belgrade, Faculty of Technology and Metallurgy, Karnegijeva 4, Belgrade 11120, Serbia, e-mails: ana_p_p@yahoo.com; mristic@tmf.bg.ac.rs; marinko@tmf.bg.ac.rs

[b]Military Technical Institute, Ratka Resanovica 1, Belgrade 11000, Serbia, e-mail: jrusmirovic@tmf.bg.ac.rs

[c]Innovation Center of the Faculty of Technology and Metallurgy Ltd., University of Belgrade, Karnegijeva 4, Belgrade 11120, Serbia, e-mail: zradovanovic@tmf.bg.ac.rs

[d]University of Defense, Military Academy, Generala Pavla Jurišića Šturma 33, Belgrade 11040, Serbia, e-mail: zlatevel@yahoo.com

[e]University of Belgrade, Faculty of Mechanical Engineering, Kraljice Marije 16, Belgrade 11120, Serbia, e-mail: vpavlovic@mas.bg.ac.rs

*Corresponding author: Jelena D. Rusmirović, Military Technical Institute, Ratka Resanovica 1, Belgrade 11000, Serbia. Tel: +381 63 8354 953. E-mail: jrusmirovic@tmf.bg.ac.rs

ABSTRACT: Novel highly effective amino-functionalized lignin-based biosorbent in the microsphere geometry (A-LMS) for removal of heavy metal ions, was synthesized *via* inverse suspension copolymerization of kraft lignin with poly(ethylene imine) grafting-agent and epoxy chloropropane cross-linker. Optimization of A-LMS synthesis, performed with respect to the quantity of sodium alginate emulsifier (1, 5 and 10 wt.%), provides highly porous microspheres **A-LMS_5**, using 5 wt.% emulsifier, with 800±80 μm diameter, 7.68 $m^2 g^{-1}$ surface area and 7.7 mmol g^{-1} of terminal amino groups. Structural and surface characteristics were obtained from Brunauer-Emmett-Teller method, Fourier Transform-Infrared spectroscopy, scanning electron microscopy, X-ray photoelectron spectroscopy and porosity determination. In a batch test, the influence of pH, **A-LMS_5** dose, temperature, contact time on adsorption efficiency of Ni^{2+}, Cd^{2+}, As(V) and Cr(VI) ions were studied. The adsorption is spontaneous and feasible with maximum adsorption capacity of 74.84, 54.20, 53.12 and 49.42 mg g^{-1} for Cd^{2+}, Cr(VI), As(V) and Ni^{2+} ions, respectively, obtained by using Langmuir model. Modeling of kinetic data indicated fast adsorbate removal rate with pore diffusional transport as rate limiting step (pseudo-second order model and Weber-Morris equations), thus further confirming high performances of produced bio-adsorbent for heavy metal ions removal.

KEYWORDS: Lignin; Microspheres; Biosorbent;

1. INTRODUCTION

Environmental pollution caused by fast growing population, urbanization and industrialization has become a serious threat to the contemporary society [1]. Heavy metal ions discharge in environment, especially in watercourses, whether uncontrolled or controlled, has become a world-wide concern because of its adverse effects, carcinogenicity and toxicity for ecosystem and human health [1,2]. Most common heavy metal ion contaminants present in water and in direct focus of this research, are nickel, cadmium, arsenate and chromate ions, originating from a wide variety of industrial processes, particularly metallurgical processes, production of nickel-cadmium batteries *etc* [3]. These heavy metals are extremely harmful to aquatic life and can be easily accumulated in the human body through the food chain and cause a variety of diseases and disorders [4,5]. In order to suppress the uncontrolled rise of water pollution by heavy metals, the US Environmental Protection Agency (EPA) limits concentration of cadmium to 0.005 ppm, arsenic to 10 ppb and of nickel and chromium to 0.1 ppm in water [6], while strict legislation mandates polluters to treat industrial effluents before discharging to watercourses [7].

Various treatment processes are explored for removing heavy metal content from industrial wastewater, such as adsorption, flocculation, ion-exchange, membrane separation, reverse osmosis, chemical precipitation, neutralization, and other often linked with expensive equipment, difficulties in implementation, toxic sludge generation or high operational costs [3,5,8]. Adsorption by porous adsorbents is considered to be a promising method for heavy metal ions removal from wastewater due to the numerous advantages compared to the other methods, such as ease of operation, high removal efficiency and selectivity, and the possibility of adsorbent regeneration/reuse [4,5,7,9]. In order to achieve all the benefits of heavy metal removal by adsorption, the key factor is the selection of a proper adsorbent coupled with its

surface design, porosity and geometry. Therefore, development of a novel, economical, high-efficient and porous adsorbent with surface active sites from natural renewable sources remains a promising method of clean-up of heavy metals and continuing area of research [3,5,8–10].

An increased interest in utilization of natural macromolecules for various high-value applications, including water purification, is present in the last decades, aiming to reduce the environmental impact, waste generation, and contribute to efficient resource use and more sustainable bio-based economy [11–14]. Natural polymers contained in woody biomass are cellulose (45-50%), hemicellulose (25-30%) and lignin (20-30%) - the most abundant aromatic biopolymer on the planet [11,14,15]. While significant progress is made in the area of applicability of hemicellulose materials in adsorption processes [5,9,16,17], lignin is still continuously researched for reaching its full potential as an eco-friendly bio-adsorbent for efficient removal of heavy-metal ions from wastewater [10,13,18–22].

Due to its complex macromolecular three-dimensional structure and presence of methoxyl, phenolic and aliphatic hydroxyl, ketone and aldehide groups, lignin has a good capacity to adsorb heavy metal ions. Several innovative modifications of lignin were also successfully tested for adsorption, such as lignin xanthate resin–bentonite clay composites [1], lignin-grafted nanocomposites [23] or lignin-based nano-traps [24], chitosan-lignin composites [7,25], chitin-lignin hybrids [26,27], lignin-based hydrogels [28–30], ion-exchange resins [21], as well as lignin-based microspheres with or without modifications [20,31–33]. Lignin microspheres, synthesized mainly through copolymerization via phenolic hydroxyl groups, have a larger surface area supporting enhanced diffusion, dispersion and mass transfer, while their chemical modification with selective functional groups represents an efficient way to improve their particular adsorption properties [31,34,35].

In this paper, we are reporting a new tailored synthesis method for amino-modified lignin microspheres (A-LMS) containing abundant amine functional groups, and used as effective and reusable adsorbent for Ni^{2+}, Cd^{2+}, As(V) and Cr(VI) ions. The scope of present study is addressed to solving modern environmental challenges *via* following subject areas: optimization of A-LMS synthesis and evaluation of adsorption performances of A-LMS in a batch system using experimental and theoretical methods. Response surface methodology (RSM) is used with several variables providing the possibility to analyze inter-relation among parameters with performing minimum of experiments [9]. In accordance with the latter, specific objectives of the current study are related to: 1) surface, textural and morphological characterization; 2) adsorption study; 3) kinetic study; 4) thermodynamic and activation parameters determination; 5) evaluating the limiting step of adsorption, and 6) reusability.

2. EXPERIMENTAL SECTION

2.1. Materials and methods

The following materials were used: epoxy chloropropane, produced by Merck Schuchardt, Germany; kraft lignin, liquid paraffin oil and poly(ethylene imine) grafting-agent (PEI), produced by Sigma-Aldrich, Germany; sodium alginate (medium viscosity), Merck, and sodium lauryl sulphate provided by Centrohem, Serbia. Single-element AAS standard solutions of nickel, cadmium, arsenic and chromium (from nitrate salts) produced by Carl Roth Gmbh Germany was used for adsorption experiments. Fourier transforms-infrared (FT-IR) spectra of the samples were recorded in absorbance mode using a Nicolet™ iS™ 10 FT-IR Spectrometer (Thermo Fisher SCIENTIFIC) with Smart iTR™ Attenuated Total Reflectance (ATR) Sampling accessories, within a range of 400-4000 cm^{-1}, at a resolution of 4 cm^{-1} and in 20 scan mode. X-

ray photoelectron (XPS) spectroscopy was used to confirm the obtained structure. XPS analyses were performed on Kratos Axis Ultra XPS system instrument. X-ray source: monochromated Aluminum K-alpha X-Ray with a source voltage of 15 kV and current of 10mA.

The particle size, distribution and morphology were observed by field emission scanning electron microscopy (FESEM) by Tescan Mira 3 FEG. FESEM micrograph of the cross section of **A-LMS_5** (Fig. S1) was used to determine minimal and maximal length of the **A-LMS_5** pores. Before analysis, microspheres were coated with Au. To evaluate A-LMS porosity, the procedure earlier described elsewhere was used [36] (Supplementary data). "Back" titration, presented in Supplementary data, was used for determination of the amine functional groups, following a procedure described earlier [37]. The specific surface area of the adsorbents was calculated according to the Brunauer-Emmett-Teller (BET), from the linear part of the nitrogen adsorption–desorption isotherms. Nitrogen adsorption–desorption isotherms were determined using a Micromeritics ASAP 2020 instrument. Samples were degassed at 100 ^{o}C for 7 h under reduced pressure. The total pore volume (V_{tot}) was given at p/p_0 = 0.98. Pore volume was calculated according to the Barrett-Joyner-Halenda (BJH) method from the desorption branch of isotherm.

The pH value of the point of zero charge, pH_{PZC}, was measured by the pH drift method. Batch adsorption and kinetic experiments of Ni^{2+}, Cd^{2+}, As(V) and Cr(VI) ions, performed at 298, 308 and 318 K and with variation of A-LMS mass, contact time (range of 5 min to 90 min) and solution pH, were applied to evaluate adsorption efficiency of A-LMS. Batch experiments were conducted to determine the effects of pH on the adsorption of heavy-metal ions in vials using 5 mL of 10 mg L^{-1} metal ion solutions at 298 K. At the end of each experiment, the solutions were filtered through 0.22-μm pore-size filters and analyzed on inductively coupled

plasma mass spectrometry (ICP-MS) system an Agilent 7500ce ICP–MS system (Waldbronn, Germany) equipped with an octpole collision/reaction cell, Agilent 7500 ICP–MS ChemStation software, a MicroMist nebulizer and a Peltier cooled (2 °C) quartz Scott-type double pass spray chamber. ICP–MS detection limit was 0.030 μg L^{-1} and the relative standard deviation (RSD) of all nickel, cadmium, arsenate and chromate species investigated after three repeating was between 1.3–5.1%. For full-scale system modeling using validated pore surface diffusion model, the adsorbent porosity was evaluated by pycnometer analysis [36].

2.2. A-LMS synthesis procedure

The inverse suspension copolymerization procedure developed by Ge *et al*. [35] was utilized, optimized with a number of modifications. Typically, 0.5 g of lignin and 10 mL deionized water were added into a three-neck flask, and 2.0 g of PEI, 0.1 g of sodium dodecyl benzene sulfonate, and 10 mL of a sodium alginate emulsifier solution (1.0 wt.%) were added into the flask while stirring. It was kept stirring for 30 min and the temperature was elevated to 60°C. Then, the above aqueous phase was added to 80 mL of liquid paraffin to form a suspension. Afterwards, 2.0 mL of epoxy chloropropane, cross-linker, was added drop-wisely and stirred for 120 min to complete the copolymerization. After centrifugation, the solid was washed three times with both petroleum ether and ethanol and finally with water, by repeating sonication/centrifugation processes, in order to remove all non-reacted compounds. A-LMS were obtained after freeze-drying for 24 h at –40 °C and further characterized. All other experiments included in the optimization procedure were performed analogously to general procedure used for A-LMS synthesis. Also, the optimization of A-LMS synthesis was performed with respect to temperature (50 and 70 ^{o}C), and a sequential collection of the products during the period 90 – 180 min at 10 min intervals. All samples were analyzed to amino group content and porosity

determination. The selected synthesized materials used in a further analysis were named as follows: A-LMS with 1.0 wt. % alginate solution – **A-LMS_1**, 5.0 wt. % – **A-LMS_5** and 10.0 wt. % – **A-LMS_10**. Creation of chemical bonding in a course of A-LMS formation is shown in Fig. 1a), and possible mechanism of complexation between Ni^{2+}, Cd^{2+}, Cr(VI), and As(V), and **A-LMS_5** surface functionalities in Fig. 1b).

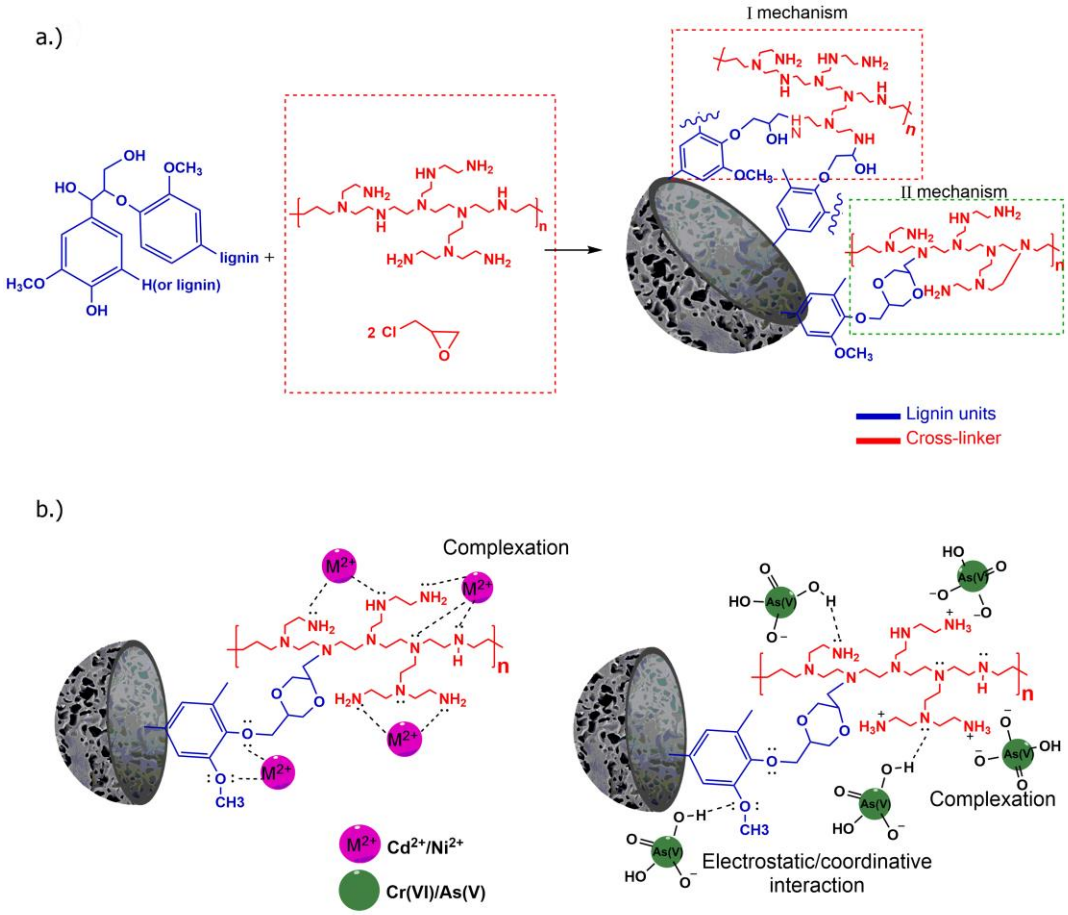

Fig. 1 Possible a) mechanism of the A_LMS microsphere formation; and b) formation of complexes with Ni^{2+}, Cd^{2+}, Cr(VI), and As(V)

Assumed cross-linking mechanism is a complex process; it includes the participation of nucleophilic substitution reactions: epoxide ring opening and two chloride exchange creating 1,4-dioxan-2,5-diyl bridging moiety (I mechanism) and concomitant/subsequent epoxide ring

opening with one chloride substitution creating 2-hydroxy-1,3-diyl moieties (II mechanism), both given on Fig. 1a). Ge et al. suggested II mechanism as the major cross-linking mechanism [35].

2.3. Experimental design and optimization

The experimental design, optimization, and analysis of variance (ANOVA), were performed to determine the simultaneous relationship between a set of experimental factors (reactants amounts and reaction time) and measure its effects on responses through the minimum number of runs. For checking the adequacy of the developed models at 95% confidence level ANOVA technique was used [38]. With Box-Behnken design surface response methodology (BBD RSM) the effects of the initial amounts of emulsifier, sodium alginate, copolymerization agent and lignin, in the polymerization mixture, and the copolymerization time, on the amino group content of the obtained A-LMS adsorbents, were investigated. Theoretical interpretations of the RSM and BBD RSM methodology and process parameters are given in the Supplementary data.

2.4. Adsorption and kinetic experiments

Batch adsorption experiments of Ni^{2+}, Cd^{2+}, As(V) and Cr(VI) ions, performed at 298, 308 and 318 K and with variation of A-LMS mass, contact time and solution pH, were applied to evaluate adsorption efficiency of A-LMS. Methodology and calculation of the adsorption capacity (Eq. S5) are provided in the Supplementary data.

3. RESULTS AND DISCUSSION

3.1. Box-Behnken design optimization results

Phase separation, sol–gel transition and phase properties depend on system reactivity, monomer solubility, phase compatibility and intermolecular interactions, which significantly influence the supramolecular structure of synthesized adsorbent. Therefore, all the synthesis parameters that influence geometry, morphology, porosity and adsorptivity (quantification of functionalities) are considered. The most influential operational parameters related to amino group content and porosity are lignin, emulsifier content, temperature and reaction time, and those were varied in the optimization procedure. The dependence of the amino group content *versus* lignin content and alginate concentration is shown on **Fig. 2**.

According to the RSM modeling results, it was found that 0.5 g of kraft lignin and 5% sodium alginate solution are optimal values used for A-LMS synthesis. The initial amount of emulsifier in the polymerization mixture was formulated in accordance, to give the desired size and porosity of A-LMS. Uniformity (particle size distribution) and sphericity were also determined. Additional optimization was performed with respect to temperature and time of reaction. Synthesis performed at lower temperature (50 ^{o}C) requested a longer time (>150 min), and opposite was true for higher temperature of 70 ^{o}C (< 100 min). In all cases, lower uniformity and sphericity of **A-LMS_5** was obtained, with pronounced lower content of amino groups for those synthesized at 70 ^{o}C. Thus, operational parameters of 60 ^{o}C and 120 min were selected. In order to further optimize the synthesis procedure, two methodologies of A-LMS adsorbent drying were applied: vacuum and freeze drying methods. According to preliminary adsorption parameters determination and higher capacity of freeze-dried **A-LMS_5** for 7-15%, this material was used in adsorption experiments. Beneficial adsorption performances of gel-type **A-LMS_5**, are due to high porosity (68%) and abundant number of amino groups (7.7 mmol g^{-1}). For checking the adequacy of the developed models at 95% confidence level ANOVA technique was

used [38]. ANOVA results follow the *F*-ratio value and all models satisfy the adequacy conditions in a non-linear form (Table S3).

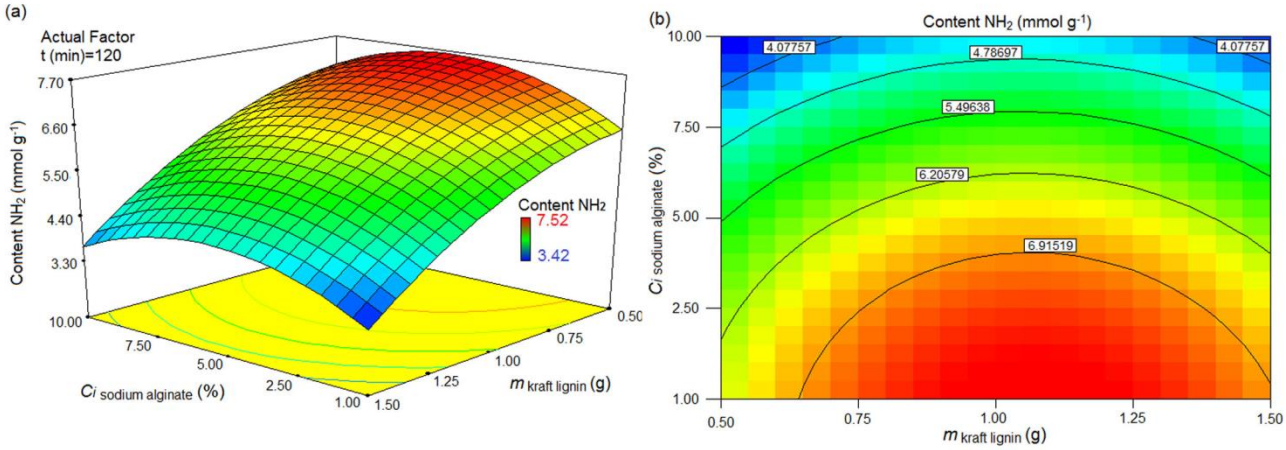

Fig. 2 3D (a) and 2D (b) plots of dependence of the amino groups content *versus* lignin content and alginate concentration

3.2. FT-IR and XPS Spectroscopy

Pure lignin sample and synthesized **A-LMS_1**, **A-LMS_5** and **A-LMS_10** were characterized using FT-IR an XPS spectroscopies (**Fig. 3**). The broad band at 3380 cm^{-1} in the lignin FT-IR spectra (Fig. 3a) is assigned to hydroxyl and phenolic O-H stretching vibration [15,39]. The bands at 1590 cm^{-1}, 1500 cm^{-1} and between 1410–1450 cm^{-1} contributed to the aromatic skeletal vibrations, indicating the aromatic structures of lignin [15,39]. Weak intensity peak at 1360 cm^{-1} is assigned to vibrations of lignin syryngyl rings and stretching vibrations of C-O bonds [15,39]. Moreover, intensive peak vibrations (1220–1260 cm^{-1}) are from guaiacyl rings [15,39]. The band at 1120 cm^{-1} originates from deformation vibrations of C-O bonds in primary alcoholic and phenolic groups [15,39]. The bands at 2842 and 2934 cm^{-1} were attributed to the symmetric and asymmetric C-H stretching vibration of methylene group [40]. However,

after copolymerization of lignin with PEI and epoxy chloropropane, some changes were noticed, associated to appearance of new absorption bands in FT-IR spectra.

Compared to lignin, the main difference of the FT-IR spectrum of A-LMS was at 1460–1025 cm^{-1}, ascribed to the stretching vibration of the C-N bond [35]. Band that originates from O-H stretching vibrations shifted to the lower wavelength (3243 cm^{-1}) and overlapped with band assigned to N-H stretching vibration (primary and secondary amines). Besides, the N-H stretching band of PEI moiety changes the shape of O-H stretching in A-LMS samples (sharp peak). For PEI-copolymerized A-LMS, the new absorption band appearing at 1460 cm^{-1} is assigned to C-N stretching vibrations [35]. Another observation is that the band at 1120 cm^{-1} for C-O bonds of primary alcohols and phenols disappeared with the concurrent appearance of new C-N group (shoulder of the peak at 1025 cm^{-1}), corresponding to the successful copolymerization between lignin, PEI and epoxy chloropropane. The bands at lower wavelengths are associated to deformation vibrations of C-H bonds in aromatic rings and N-H out-of-plane bending vibration (band observed at 856 and 740 cm^{-1}) [15,39].

A comparison of the percentage share of the individual elements in different samples (based on the XPS Survey spectrum – Table S4 and S5 – Supplementary data) and the values of the positions and the areas of the separate components were analysed. Deconvolution of C 1s spectrum of lignin (**Fig. 3c**)) shows two clearly expressed peaks at 284.8 and 286.2 eV, which correspond to carbon in C-C or C-H bonds [41–43], and to C-O or C-OH bonds [41,43], respectively. A weak peak observed at 288.2 eV originates from carbonyl C=O or O-C-O group. The intensities of the peaks, which refer to the oxygen-containing groups in the C 1s spectra, are largely reduced in the samples **A-LMS_1-5**, indicating the lower content of C-O bonds. The occurrence of the prominent component at 285.8 eV in the **A-LMS_10** spectrum may be a

consequence of enhanced formation of C-N bonds [43,44]. The peaks obtained by deconvolution of the O1s spectrum (**Fig. 3d**) for lignin sample, with positions at 531.8 and 533.2 eV, correspond to C=O and C-O bonds, respectively [41]. The analysis of all O1s spectra confirms the conclusions derived from the C1s spectra: contribution of C-O bonds obviously decreases for the samples **A-LMS_1-5**, and increase for the **A-LMS_10**.

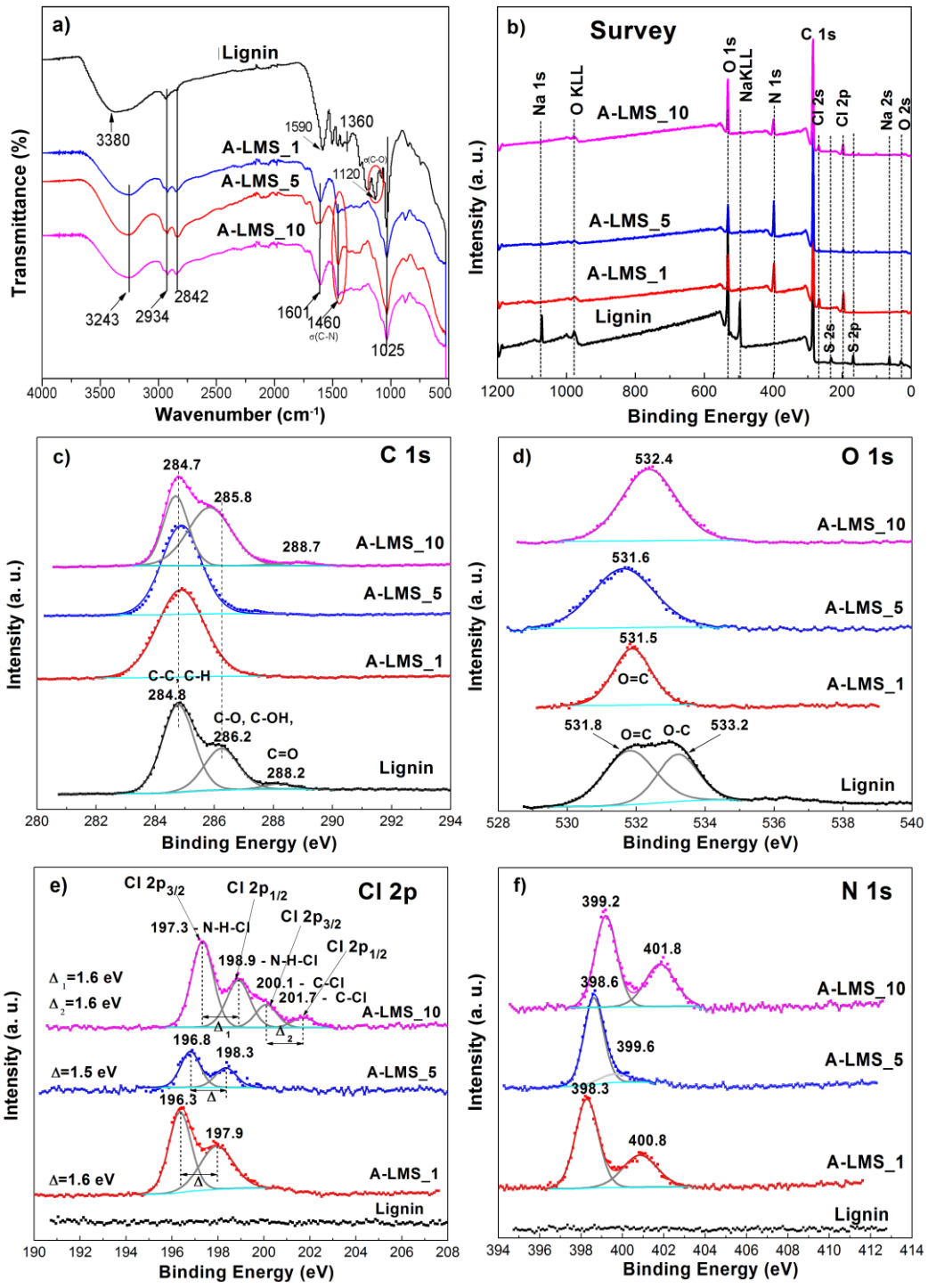

Fig. 3 FT-IR and XPS spectra of lignin and synthesized **A-LMS_1**, **A-LMS_5** and **A-LMS_10**: a) FTIR, b) Survey, c) C1 s, d) O 1s, e) Cl 2p, f) N 1s (Label Δin Fig. 3d stands for the difference: $BE(2p_{1/2})$-$BE(2p_{3/2})$)

The occurrence of the peaks in Cl 2p spectrum (**Fig. 3e**) is noticed only for the **A-LMS_1-10** samples. The spin-orbital splitting into Cl $2p_{3/2}$ and Cl $2p_{1/2}$ components is observed, where the difference between the $2p_{1/2}$ and $2p_{3/2}$ components of the each considered bond remains close to the expected value of 1.6 eV. In Fig. 3e the value Δ_1 refers to the difference between the position of the $2p_{1/2}$ and $2p_{3/2}$ components of the first type of bond (Cl $2p_{3/2}$ belongs to the region of 196.3-197.3 eV), while the value Δ_2 represents the difference between the positions of the $2p_{1/2}$ and $2p_{3/2}$ components of the second type of bond (Cl $2p_{3/2}$ takes the value of ~ 200.1 eV). According to the literature data, the peak of $2p_{3/2}$ component at 196.3-197.3 eV can be attributed to the chloride anion [45], or to N-H-Cl bond, while the peak of $2p_{3/2}$ component at 200.1 eV can originate from the chlorine covalently bonded to sp^2 carbon [46]. It can be noticed that the last mentioned peak and analogous $2p_{1/2}$ component at 201.7 eV are prominent only in the sample with the highest percentage of added sodium alginate.

The obtained N 1s spectra (**Fig. 3f**) indicate the existence of a few types of nitrogen states in the **A-LMS_1-10** samples, where the first peak (398.3-399.2) may originate from the contribution of imine and amine type of nitrogen, while the peaks at 400.8-401.8 eV can be interpreted as oxidized amine and protonated amine/imine nitrogen [47].

3.3. Morphological and textural properties

Since the formulation of an emulsion mixture has a profound effect on the textural/morphological properties of the copolymerized samples, the effect of the sodium alginate solution concentration (emulsifier) on morphology, textural properties, size and shape of the synthesized **A-LMS_1-10** was analyzed. As the emulsifier stabilizes the growing microsphere surface, the concentration of the emulsifier in the polymerization mixture

determines the nucleation of new particles [48], prevents aggregation/flocculation and coalescence.

The FESEM micrographs (**Fig. 4**) revealed small, irregularly coral shaped and agglomerated **A-LMS_1** (**Fig. 4a** to **c**), with the 20-80 μm diameter. It could be explained by the suspension instability due to low emulsifier concentration (≤1.0 wt.%), and droplet separation under the performed mixing condition [49], that produced lower irregular particles. Moreover, the lower polymerization rate causes the formation of partially porous surface (22%) of the **A-LMS_1** with mostly closed pore system (**Fig. 4c**). With the increase of emulsifier concentration, the increase in the polymerization rate and formation of highly porous regular spherical shape is observed (**A-LMS_5**, **Fig. 4d** to **f**). The **A-LMS_5** sample shows the highest porosity (68%) indicating optimal copolymerization conditions (emulsifier content) that enable high level of polymerization rate. It can be attributed to the increase of the suspension stability and the duration of nucleation with increasing the emulsifier concentration [48,49]. This is explained by the fact that the higher emulsifier level produces the greater number of monomer chains (lignin, PEI and epoxy chloropropane) that can be initiated, thus the monomer concentration decreases by dilution of the alginate emulsifier [48,49].

The mean diameter of **A-LMS_5**, determined by KVI Popovac software, is approximately 800±80 μm. Apparently, utilization of 5.0 wt.% or 10.0 wt.% of emulsifier doesn't significantly contribute to the A-LMS shape and size. The opposite is found for porosity. Lower porosity of **A-LMS_10** sample, 48%, confirms negative effect of inadequate amount of alginate emulsifier in the copolymerization mixture. The minimal and maximal pore diameters of the **A-LMS_5** samples are approximately 0.12 μm and 3.06±0.04 μm, respectively.

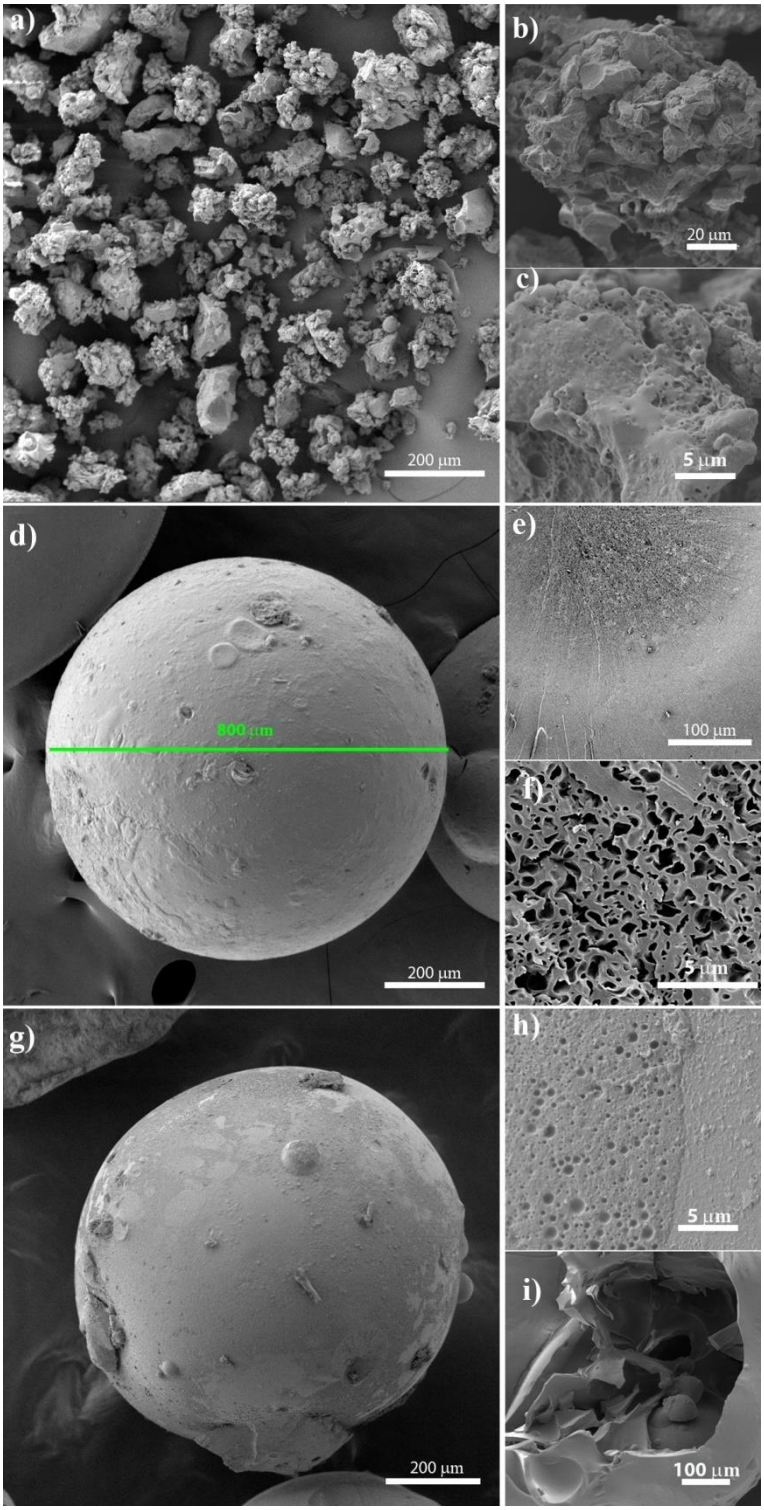

Fig. 4 FESEM micrographs of **A-LMS_1** (a, b, c), **A-LMS_5** (d, e, f) and **A-LMS_10** (g, h, i)

Specific surface area (S_{BET}), pore volume (V_{total}), volume of mesopores (V_{meso}), average pore diameter (D_{mn}), and pore diameter (D_{max}) of **A-LMS_1-10** samples are determined using BET/BJH method and obtained results are presented in Table S6. The S_{BET} value of **A-LMS_1** (1.36 $m^2 g^{-1}$) is lower than S_{BET} of lignin (1.8 $m^2 g^{-1}$) [35]. With the increase of alginate emulsifier concentration the increase in S_{BET} values (7.68 $m^2 g^{-1}$ for **A-LMS_5**), volumes of total pore and mesopores diameter is observed. The increased S_{BET} value of the **A-LMS_5** (4.27 times higher than S_{BET} of lignin) is beneficial to the adsorption of heavy metals from water [35]. With the goal of achieving higher adsorption capacities, large number of amino-groups was introduced using PEI reactant. High amino-group content in synthesized lignin microspheres was found to be 7.7 and 6.5 to mmol g^{-1} for **A-LMS_5** and **A-LMS_10**, respectively (Table S6).

3.4. Determination of the pH_{PZC} of A-LMS_5 adsorbent and effect of pH on adsorption efficiency

Except of the A-LMS morphology/textural characteristic, the operational conditions, such as acid/base conditions, electronegativity and proton donating/accepting capability may be responsible for the effectiveness of heavy metal removal [31]. The pH influences the state of equilibrium of heavy metal ionic/oxyanion species and protonation/deprotonation of A-LMS surface groups [50]. Value of electrostatic attractive forces between heavy metal ion/oxyanion and A-LMS surface charges/functionalities affects the adsorption efficiency [51,52]. In aqueous solution, the A-LMS interior/exterior surface is covered with amino ($-NH_2$) groups that can be protonated/deprotonated, and thus existing as $-NH_3^+$, NH_2 or $-NH^-$. Their pH-dependent behavior is defined by pH dependent boundary charges and pH_{PZC} value, as the point at which equilibration of protonation/deprotonation processes takes place [31], *i.e.* the surface concentrations of $-NH_3^+$ and $-NH^-$ groups are equal. The determined pH_{PZC} of **A-LMS_5** was

6.2 (Fig. S4). As an initial step, pH dependent ionization of Ni^{2+} and Cd^{2+} ions and As(V) and Cr(VI) oxyanions was calculated using MINTEQ 3.0 software [53], and obtained results indicate that high removal efficiencies in the pH region of 6-8 would be expected (Fig. S5). In order to check such presumption, the removal degree of targeted ions/oxyanions *versus* the initial pH (pH_i) was studied. At pH lower then pH_{PZC}, surface of **A-LMS_5** is positively charged and mostly covered with $-NH_3^+$. Therefore, the **A-LMS_5** shows low adsorption efficiency for bivalent positively charged Ni^{2+} and Cd^{2+} ions due to the repulsive electrostatic forces. On the contrary, multiple bonding interactions of As(V) and Cr(VI) mono- and di-valent oxyanions with ammonium groups indicate significant potential of synthesized **A-LMS** to be used at this pH. Percentage uptake of the Cd^{2+} and Ni^{2+} ions increases with an increase in pH from 4 to 8. In the 6-8 pH range, the maximum uptake (close to 100%) of Ni^{2+} and Cd^{2+} ions is observed. Furthermore, adsorption capabilities at pH>8 could originate from additional contribution of the precipitation of insoluble metal hydroxides [54]. Thus, adsorption curves for studied cations represent only adsorption with excluded precipitation at pH>8. According to this, at pH<8, it could be accepted with high degree of certainty that removal of Cd^{2+} and Ni^{2+} was not affected by hydroxide/salt precipitation giving appropriate results and conclusions [54]. In this sense, the selection of pH 6.5 for Cd^{2+} and Ni^{2+} removal and pH 6.0 for both Cr(VI), considering CrO_4^{2-} /$HCrO_4^-$ ions, and As(V), taking into account $HAsO_4^{2-}$/$H_2AsO_4^-$ ions, was a justified selection of adsorption parameters to achieve high adsorption capacities. Influence of pH on Cd^{2+}, Ni^{2+}, $HAsO_4^{2-}$/$H_2AsO_4^-$ and CrO_4^{2-}/$HCrO_4^-$ ions removal by **A-LMS_5** is shown on **Fig. 5.**

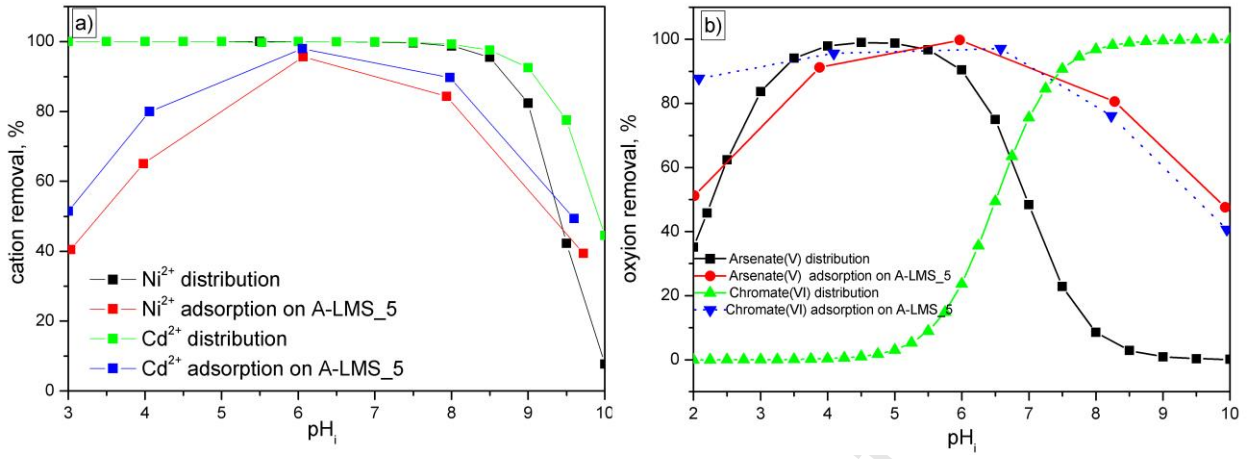

Fig. 5 Influence of pH on Cd^{2+}, Ni^{2+}, $HAsO_4^{2-}/H_2AsO_4^-$ and $CrO_4^{2-}/HCrO_4^-$ ions removal by **A-LMS_5** (C_i = 1 g L^{-1}, m/V = 1 g L^{-1}, T = 308 K)

3.5. Adsorption/desorption study of Cd^{2+}, Ni^{2+}, $CrO_4^{2-}/HCrO_4^-$ and $HAsO_4^{2-}/H_2AsO_4^-$ removal on A-LMS_5

After determination of morphology and amino-group content of the synthesized lignin microspheres, **A-LMS_5** was chosen as the most appropriate for adsorption experiments. It was demonstrated that Cd^{2+} ions form cyclic and non-cyclic complexes with amine containing molecules by using relativistic effective core potentials [55]. Other study demonstrated that the adsorption process of heavy metals on hybrid amino-modified adsorbent was dominated by formation of strong surface complexation with nitrogen atom and electrostatic/coordinative interaction with oxygen atom [56]. Moreover, it was confirmed that heavy metals undergo complexation and hydrolysis during adsorption [50,57]. Formation of cyclic and non-cyclic complexes between Cd^{2+} and Ni^{2+} and **A-LMS_5** surface groups occur in a similar manner, as presented in **Fig. 1**. However, analysis of adsorption mechanism of oxyanions is of a higher complexity, and depends on operational pH [50,57]. At operational pH 6, the protonated amine groups, *i.e.* $-NH_3^+$, on the **A-LMS_5** surface are responsible for $CrO_4^{2-}/HCrO_4^-$ and $HAsO_4^{2-}$

/$H_2AsO_4^-$ species adsorption to a large extent [58]. The protonated amine groups create complexes with $HAsO_4^{2-}$/$H_2AsO_4^-$ and CrO_4^{2-}/$HCrO_4^-$ oxyanions (major species) *via* electrostatic attraction [58]:

$–NH_3^+ + H_2AsO_4^- \rightarrow –NH_3^+$---- $HAsO_4^{2-}/H_2AsO_4^-$

$–NH_3^+ + HCrO_4^- \rightarrow –NH_3^+$---- $CrO_4^{2-}/HCrO_4^-$

In addition, different proton-donating/proton-accepting interactions of amino group (N-H proton and lone electron pair, respectively) with pH-dependent ionized species: dihydrogen- and hydrogen arsenate and chromate could be established. At pH 6, $HAsO_4^{2-}/H_2AsO_4$ are present, which indicates the possibility for creation of different hydrogen bonding interactions, as presented on **Fig. 1b**.

The Langmuir, Freundlich, Temkin and Dubinin-Radushkevich isotherm models are given by Eqs.S6-9 (Supplementary data). Adsorption thermodynamic parameters are estimated using the Gibbs free energy equation (Eq.S10) and the linearized van′t Hoff equation (Eq.S11), *i.e.*, the van′t Hoff plot. Langmuir, Freundlich, Temkin and Dubinin-Radushkevich adsorption isotherm fitting data (298, 308 and 318 K) for all studied ions are presented in **Table 1 and Fig. S7**.

Table 1 Non-linear Langmuir, Freundlich, Temkin and Dubinin-Radushkevich isotherm parameters for Cd^{2+}, Ni^{2+}, $HAsO_4^{2-}/H_2AsO_4^-$and $CrO_4^{2-}/HCrO_4^-$ ions adsorption on **A-LMS_5**

			Langmuir				
		Cd^{2+}			Ni^{2+}		
	T(K)	q_e (mg g^{-1})	K (l mg^{-1})	R^2	q_e (mg g^{-1})	K (l mg^{-1})	R^2
A-LMS_5	298	60.95±1.22	2.89±0.05	0.98	46.79±0.64	1.17±0.02	0.98
	308	65.56±1.97	3.41±0.08	0.98	48.03±0.89	1.23±0.03	0.98
	318	74.84±2.91	4.05±0.11	0.97	49.42±1.34	1.55±0.05	0.99
		$HAsO_4^{2-}/H_2AsO_4^-$			$HCrO_4^-/CrO_4^{2-}$		
	T K)	q_e (mg g^{-1})	K (l mg^{-1})	R^2	q_e(mg g^{-1})	K (l mg^{-1})	R^2
	298	49.23±0.84	2.36±0.09	0.98	50.72±0.94	2.47±0.09	0.99
A-LMS_5	308	50.53±1.74	2.57±0.12	0.98	51.76±1.14	2.56±0.08	0.99
	318	53.12±1.66	2.91±0.11	0.99	54.20±1.43	2.86±0.11	0.99

Freundlich

	Cd^{2+}				Ni^{2+}			
	T(K)	K_f ($mol^{1-n}L^n/g$)	*1/n*	R^2	K_f ($mol^{1-n}L^n/g$)	*1/n*	R^2
A-LMS_5	298	37.32±1.45	0.40	0.99	21.24±0.63	0.45	0.99
	308	42.85±1.95	0.41	0.99	22.20±0.95	0.44	0.99
	318	52.63±2.68	0.44	0.99	25.42±1.05	0.44	0.98
	$HAsO_4^{2-}/H_2AsO_4^-$				$HCrO_4^-/CrO_4^{2-}$		
	T (K)	K_f ($mol^{1-n}L^n/g$)	*1/n*	R^2	K_f ($mol^{1-n}L^n/g$)	*1/n*	R^2
	298	27.92±0.85	0.36	0.99	29.38±1.05	0.38	0.99
A-LMS_5	308	29.48±0.93	0.37	0.99	30.29±1.17	0.38	0.99
	318	32.80±1.35	0.38	0.99	33.49±1.25	0.39	0.99

Temkin

	Cd^{2+}					Ni^{2+}			
	T(K)	A ($L\ g^{-1}$)	*b*	B ($J\ mol^{-1}$)	R^2	A ($L\ g^{-1}$)	*b*	B ($J\ mol^{-1}$)	R^2
A-LMS_5	298	58.61±0.89	256.97	9.65±0.29	0.94	16.04±0.24	285.6	8.68	0.97
	308	68.92±0.98	247.75	10.34±0.36	0.93	17.75±0.34	293.25	8.74	0.96
	318	80.68±3.23	228.80	11.56±0.45	0.92	20.51±0.64	282.45	9.36	0.98
	$HAsO_4^{2-}/H_2AsO_4^-$					$CrO_4^{2-}/HCrO_4^-$			
	T(K)	A ($L\ g^{-1}$)	*b*	B ($J\ mol^{-1}$)	R^2	A ($L\ g^{-1}$)	*b*	B ($J\ mol^{-1}$)	R^2
A-LMS_5	298	55.88±0.91	328.63	7.82±0.19	0.94	49.45±0.99	304.16	8.15	0.96
	308	55.48±0.89	323.25	7.78±0.22	0.95	52.69±1.71	311.11	8.23	0.95
	318	55.52±1.29	303.76	7.67±0.09	0.97	53.33±1.91	295.36	8.96	0.96

Dubinin-Radushkevich

	Cd^{2+}					Ni^{2+}			
	T(K)	q_m ($mg\ g^{-1}$)	K_{ad} ($mol^2\ KJ^{-2}$)	E_a (KJ mol^{-1})	R^2	q_m ($mg\ g^{-1}$)	K_{ad} ($mol^2\ KJ^{-2}$)	E_a (KJ mol^{-1})	R^2
A-LMS_5	298	36.28±1.42	8.04±0.12	7.89	0.87	27.99±0.89	7.65±0.11	8.08	0.87
	308	39.12±1.57	7.96±0.19	7.92	0.88	28.90±0.94	7.62±0.15	8.10	0.88
	318	43.68±1.65	7.85±0.22	7.98	0.89	32.35±1.29	7.50±0.21	8.16	0.89
	$HAsO_4^{2-}/H_2AsO_4^-$					$CrO_4^{2-}/HCrO_4^-$			
	T(K)	q_m ($mg\ g^{-1}$)	K_{ad} ($mol^2\ KJ^{-2}$)	E_a (KJ mol^{-1})	R^2	q_m ($mg\ g^{-1}$)	K_{ad} ($mol^2\ KJ^{-2}$)	E_a (KJ mol^{-1})	R^2
A-LMS_5	298	30.21±1.21	7.82±0.35	7.99	0.86	31.68±0.82	7.40±0.41	8.22	0.87
	308	31.38±1.43	7.78±0.29	8.02	0.86	31.88±0.96	7.40±0.36	8.22	0.86
	318	34.86±1.50	7.67±0.27	8.07	0.89	35.11±1.35	7.30±0.29	8.27	0.88

High adsorption capacity (q_e), obtained using Langmuir isotherm model (**Table 1**), increases with the temperature increase. Moreover, slightly higher values of the Langmuir constant (K), that reflect the sorption affinity, were obtained for Cd^{2+}, $CrO_4^{2-}/HCrO_4^-$ and $HAsO_4^{2-}/H_2AsO_4^-$ ions at all temperatures. This can be attributed to the slightly lower atomic radius of Cd^{2+} ions and higher probability of surface complexation of $CrO_4^{2-}/HCrO_4^-$ and $HAsO_4^{2-}/H_2AsO_4^-$ oxyanions, compared to Ni^{2+} ions. Also, comparison of the adsorption performances of lignin indicates the benefits of **A-LMS_5** synthesis: 46.2, 31.4, 12.6 and 14.3 mg g^{-1} for Cd^{2+}, Ni^{2+}, $CrO_4^{2-}/HCrO_4^-$ and $HAsO_4^{2-}/H_2AsO_4^-$ ions, respectively.

The formation of coordination complexes of studied ions with A-LMS is confirmed using FT-IR spectroscopy (**Fig. 6**). Analytical statistics - testing the hypotheses about the significance of the isothermal model was performed by analyzing variance ANOVA in the software package Origin 8 and results are presented in **Table S7**. Based on the P-value (probability), we obtained which model has the highest significance. The P value indicates that the result is correct or incorrect. If P value is less than 0.05 (or 0.01) that indicates that the probability of random and incorrect results is less than 5% (1%). The lowest P values in the Freundlich isothermal model indicate that this model has the lowest probability of random and inaccurate results, or that correlates with the experimental data. The value "Pred R-Squared" and "Adj R-Squared" is in reasonable agreement with the P-value obtained by analysis of variance ANOVA.

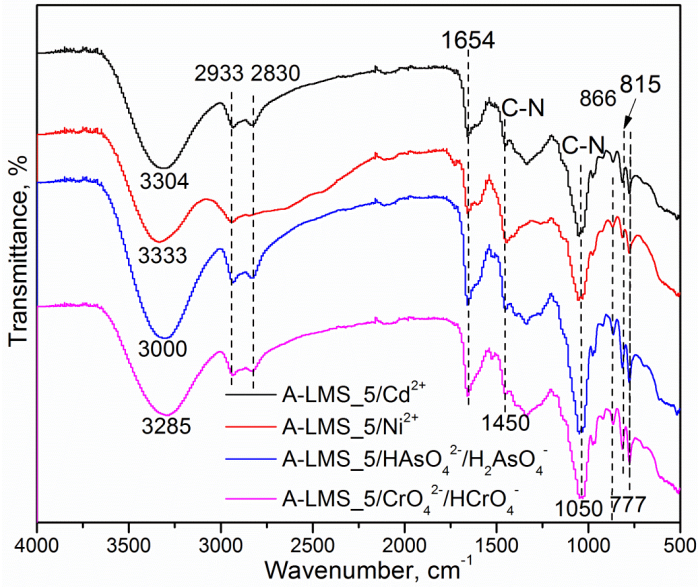

Fig. 6 FTIR spectrum of **A-LMS_5** after adsorption

When comparing the FT-IR spectra of **A-LMS_5** before and after adsorption, it is observed that the C–N band signal in 1460 cm^{-1} region is reduced, while band at 1025 cm^{-1} increased in wavelength after adsorption, indicating that amino linkages are weakened during adsorption processes. In general, in the whole region from 1650-1000 cm^{-1} significant changes of peak structure (intensity change and position shift) indicate that lignin functionalities and amino groups participate in cations/oxyanions binding. Moreover, a significant increase of N-H out-of-plane bending vibration is observed (region 866 – 777 cm^{-1}), corresponding to the electrostatic interaction/coordination of either cations or oxyanions/**A-LMS_5**. Increased intensity of these vibrations arise from cations/lone electron pair and oxyanions/hydrogen interactions causing bond force change, and thus changes of the mode of out-of-plane vibration of amino group coordinated with ions is a consequence. Furthermore, the Langmuir isotherm assumes that mechanism of adsorption of ions onto amino-functionalized **A-LMS_5** adsorbent can be attributed to the monolayer adsorption with equal enthalpy and energy for all adsorption reactive

centers. According to it, the energy of adsorption is generally considerably larger than for the second or higher layers, while formation of multilayer is less possible [59]. The values of the Freundlich parameter (*1/n*) are lower than 1 and slightly different for all studied ions, which implies chemisorptions [60].

Thermodynamic parameters of removal of Cd^{2+}, Ni^{2+}, $HAsO_4^{2-}/H_2AsO_4^-$ and $CrO_4^{2-}/HCrO_4^-$ ions on **A-LMS_5** adsorbent are shown in **Table 2**. The negative change of free energy ($\Delta G°$) in the range of -45.08 to -37.56 kJ mol^{-1} for all studied ions/oxyanions indicate that adsorption occurs *via* spontaneous reactions followed by both physisorption and chemisorption mechanisms [37,50,61,62]. Slightly $\Delta G°$ increase (absolute value) with temperature increase indicates that desolvation and diffusion processes are more feasible at higher temperatures [50]. The endothermic nature of adsorption for all studied ions is confirmed by the positive enthalpy change ($\Delta H°$) (**Table 2**) [63]. Higher $\Delta H°$ values, obtained for adsorption of $HAsO_4^{2-}/H_2AsO_4^-$ and $CrO_4^{2-}/HCrO_4^-$ oxyanions, indicate higher contribution of hydration on the $H_2AsO_4^-/HCrO_4^-$/**A-LMS_5** surface, and lower extent of diffusional processes [50].

Table 2 Thermodynamic parameters Cd^{2+}, Ni^{2+}, $HAsO_4^{2-}/H_2AsO_4^-$ and $CrO_4^{2-}/HCrO_4^-$ ions obtained at 298, 308 and 318 K using **A-LMS_5** adsorbent

	Cd^{2+}				**Ni^{2+}**		
	T (K)	ΔG^o (kJ mol^{-1})	ΔH^o (kJ mol^{-1})	ΔS^o (J mol^{-1} K^{-1})	ΔG^o (kJ mol^{-1})	ΔH^o (kJ mol^{-1})	ΔS^o (J mol^{-1} K^{-1})
A-LMS_5	298	-41.42	13.23	183.28	-37.56	11.03	162.73
	308	-43.23			-38.95		
	318	-45.08			-40.82		
	$HAsO_4^{2-}/H_2AsO_4^-$				**$CrO_4^{2-}/HCrO_4^-$**		
	T (K)	ΔG^o (kJ mol^{-1})	ΔH^o (kJ mol^{-1})	ΔS^o (J mol^{-1} K^{-1})	ΔG^o (kJ mol^{-1})	ΔH^o (kJ mol^{-1})	ΔS^o (J mol^{-1} K^{-1})
A-LMS_5	298	-39.90	8.34	161.74	-39.12	5.79	150.51
	308	-41.46			-40.52		
	318	-43.14			-42.13		

Low endothermic nature of Cd^{2+} and Ni^{2+} ions adsorption is due to low energy released by desolvation of Cd^{2+}/Ni^{2+}cations and established Cd^{2+}/ and Ni^{2+}/**A-LMS_5** interactions [50]. Increase in randomness (disorder) on boundary solid-liquid surface [50], and other processes, such as hydration/dehydration and ion exchange at adsorbent surface, could be contributing factors to positive values of entropy change ($\Delta S°$). Higher $\Delta S°$ for Cd^{2+}/Ni^{2+} adsorption is due to water release from arranged structure of tightly bonded Cd^{2+}/Ni^{2+} with hydration shell [50]. In the course of adsorption, concentration of the adsorbate on the surface is accompanied by a decrease in configurational entropy of bonded species. This phenomenon is of higher significance for oxyanions. The ions/**A-LMS_5** interfacial interactions and formation of coordinating complexes (**Fig. 1**) leads to appropriate decrease in all type of motions (translational, rotational and vibrational), which contribute to entropy decrease. Value of $\Delta S°$ change depends on the extent of ion/amino group interactions, *i.e.* on the charge *versus* radius of ion and proton-donating/accepting properties of amino group. In general, both mode and extent of coordination of the cations/oxyanions on **A-LMS_5** and conformational effect, contribute to increase of the orderliness of cation/**A-LMS_5** system, *i.e.* higher $\Delta S°$ was obtained.

The **A-LMS_5** adsorbent was used in a preliminary optimization of the desorption study by varying concentration and regenerator type. Production of high performance adsorbent and development of optimal desorption technology contribute to decrease of exhausted adsorbent and wastewater generation. Efficiency of cation desorption increase with pH increase, and both sodium hydroxide and sodium hydrogen carbonate are applicable to provide >92% bonded cation release. Desorption study performed using acidic regenerator, *e.g.* hydrochloric, oxalic or citric acid also show high desorption efficiency (>90%). Proton donating ability of acidic regenerator cause concomitant protonation of amino group; activation of the adsorbent using basic solution

was necessary to restore **A-LMS_5** adsorption potential after desorption cycle. Similar results were obtained for oxyanions. Thus, the most useful desorption system, 4% $NaHCO_3$ and 2% NaCl, was used throughout desorption study.

Reusability study results show low decrease of adsorption efficiency (approximately, 21 %, 20 %, 26 % and 19 %) after three repeated adsorptions/desorption cycles for Cd^{2+}, Ni^{2+}, $HAsO_4^{2-}$ /$H_2AsO_4^-$ and CrO_4^{2-}/$HCrO_4^-$ ions, respectively. Obtained results indicate that the applied synthesis method for A-LMS provided the adsorbent with a high degree of removal efficiency of Cd^{2+}, Ni^{2+}, $HAsO_4^{2-}$/$H_2AsO_4^-$and CrO_4^{2-}/$HCrO_4^-$ ions from water solution, able to be used in three cycles (adsorption/desorption), thus providing a safe technology for water purification.

Together with the regeneration as one parameter related to cost-efficiency, *i.e.* longevity related to the effective number of adsorption/desorption cycles, the competitive adsorption also provides an information on the affinity; it describes the adsorbent potential to remove appropriate pollutant in a presence of other common ions found in natural water (exploitation period). Water from the irrigation channel near to the city of Zrenjanin in Serbia was used in a competitive study for cations/anions removal using **A-LMS_5**. Prior to adsorption, aeration was undertaken in order to oxidize As(III) and Cr(III) to higher oxidation state. Competitive adsorption was performed by spiking of collected water with 100 μg L^{-1} of Cd^{2+}, Ni^{2+}, As(V) and Cr(VI) ions. Obtained results are given in **Table 3**, and showed satisfactory pollutant removal efficiency with low selectivity. Obtained results showed low affinity with respect to ions present in real water, and removal efficiency/capacity depends on both valence state of cations/oxyanions and concentration. The largest interference on the efficiency of ions of interest were seen by Fe^{3+} and Al^{3+} hard acids, and one borderline acid Pb^{2+}, as a result of higher affinity with respect to the amino group, in comparison to medium strong acid Ni^{2+} and soft acid Cd^{2+} ion. Other interferences of competitive

anions/oxyanions were low, which means that the highest influence of electrostatic interactions and strength of binding interactions to removal efficiency could be noticed. Prior to adsorption, humic acid and organic materials (NOM) were removed, as it showed the highest detrimental effect to decrease of adsorption efficiency. In the future research, applicable technology for humic acid/NOM removal will be designed to be performed in the first step to preserve high performance of **A-LMS_5** for ions removal.

Table 3 The pollutant removal by **A-LMS_5** from real water sample (pH ~ 6.4)

Irrigation water before treatment		**Irrigation water after treatment**	
ions	**mg L^{-1}**	**mg L^{-1}**	**removal %**
Pb^{2+}	7.9	0.8	90
Fe^{3+}	17.4	1.1	94
Al^{3+}	2.2	0.4	82
Ca^{2+}	72	52.4	27
Mg^{2+}	16	9.1	43
Cd^{2+}	0.15	0.004	97
Ni^{2+}	0.19	0.02	89
Zn^{2+}	102	86	16
Cr(VI)	0.18	0.01	95
As(V)	0.22	0.009	96
SO_4^{2-}	57	53	7
Cl^-	32	31	3

Satisfactory efficiency and low selectivity of the used adsorbent was obtained. At experimental conditions (m/V = 0.5 g L^{-1}, T = 298 K) remaining concentration of pollutants of interest was below maximum permissible concentrations (MPC) in drinking water prescribed by EPA, i.e. <0.1 mg L^{-1} for Cr(VI), <0.01 mg L^{-1} for As(V) and <0.005 mg L^{-1} for Cd^{2+} or WHO, i.e. <0.07 mg L^{-1} for Ni^{2+}, <0.05 mg L^{-1} for Cr(VI), <0.01 mg L^{-1} for As(V).

3.6. Monolayer model for single-compound adsorption

For the monolayer model for single-compound adsorption, it is assumed that heavy metal ions/oxyanions are adsorbed with one energy (-ε) [64]. The –ε describes the interaction of ions with the surface of **A-LMS_5**. Adsorption energy is calculated according to the equations presented in the Supplementary Data, and the partition function of one identical site and the monolayer model for single-compound adsorption are also described. General Langmuir model interpretation was followed, where each adsorption site accommodates one ion following chemical pseudo-reactions (Eqs. S11-S13) [65,66]. The determination of the number of ions that interact with one receptor site offers reliable information: if the number of the bonded/complexed ions/oxyanions per site is lower than 1, the ions interact with at least two receptor sites (multi-link); if the *n* is higher than 1, the receptor site is occupied by minimum one ion [65]. For all investigated single-compound systems, the higher values of *n* are obtained. It confirms that the main adsorption mechanism of studied ions occur *via* complexation with nitrogen atom and electrostatic/coordinative interaction with oxygen atom. Increase of *n* values, together with the temperature increase, was observed for Ni^{2+}, $HAsO_4^{2-}/H_2AsO_4^-$ and $HCrO_4^-/CrO_4^{2-}$ ions, following the increase of the adsorption capacity (Table S10). The opposite is found for Cd^{2+} ions, where the highest values of *n* is obtained at 298 K. Lower values of *n*, but still higher than 1, are found for the Cd^{2+} and Ni^{2+} indicating different adsorption mechanism in relation to $HAsO_4^{2-}/H_2AsO_4^-$ and $HCrO_4^-/CrO_4^{2-}$oxyanions.

3.7. Adsorption kinetic study of Cd^{2+}, Ni^{2+}, $CrO_4^{2-}/HCrO_4^-$ and $HAsO_4^{2-}/H_2AsO_4^-$ adsorption on A-LMS_5

Time dependent adsorption study was performed in a batch system and the obtained experimental data fitted using different kinetic rate equations (Eqs. S18-22) [67]; the results of a kinetic study with the following models: i) Pseudo Second Order (PSO), ii) Roginsky-Zeldovich-Elovich (Elovich), (iii) Dunwald-Wagner (DW), iv) Homogenous Solid Diffusion (HSDM), are presented in **Table 4**. Intra-particular Weber-Morris (W-M) Model results are shown in **Table 5**.

The kinetic parameters show that **A-LMS_5** possesses high affinity with respect to studied ions, and satisfactory rate at which system attains equilibrium and that PSO kinetic model can be used for the prediction of the adsorption kinetics of studied ions on A-LMS. Considering the PSO kinetic law, the rate limiting step is related to chemical adsorption involving valence forces through sharing or the exchange of electrons between the sorbent's reactive sites and metal cations [23,68] (complexation/coordination with **A-LMS_5** nitrogen atom and electrostatic/coordinative interaction with oxygen atom). The analysis of kinetic data at different temperature, using PSO model, resulted in insignificant k_2 values increase with the temperature increase. The highest values of k_2 constant and q_e are obtained at 318 K. It indicates that higher energetic input contributes to a more efficient complexation of studied cations, than for anions, with adsorbent reactive sites (increased contribution of chemisorption) and more intensive/efficient diffusional ions transport at higher temperatures. Low activation energy (E_a) values indicate that the adsorption is diffusion-controlled process [69]. The higher E_a for the adsorption of oxyanions reflect the significance of adsorbent morphology/porosity and ionic radius to higher energy demand.

Table 4 Fitted kinetic data for the adsorption of studied pollutants on **A-LMS_5** [$C_{i\,[Cd^{2+},\ Ni^{2+}]}$= 10 mg L^{-1}, pH = 6.5; $C_{i\,[As(V),\ Cr(VII)]}$= 10 mg L^{-1}, pH = 6.0, m/V = 1 g L^{-1}]

Kinetic model	T (K)	Constants	Cd^{2+}	Ni^{2+}	CrO_4^{2-} /$HCrO_4^-$	$H_2AsO_4^-$ /$HAsO_4^{2-}$
PSO	*298*	$k_2 \cdot 10^2$ (g mg^{-1} min^{-1})	1.477	0.969	1.735	0.753
		R^2	0.997	0.997	0.999	0.997
	308	$k_2 \cdot 10^2$ (g mg^{-1} min^{-1})	1.566	1.028	1.951	0.858
		R^2	0.997	0.998	0.999	0.994
	318	$k_2 \cdot 10^2$ (g mg^{-1} min^{-1})	1.668	1.134	2.173	0.975
		R^2	0.998	0.998	0.999	0.996
		E_a (KJ mol^{-1})	4.781	6.167	8.452	10.133
Elovich	*298*	α^* (mg g^{-1} min^{-1})	2.56	1.45	3.97	1.29
		β^* (mg g^{-1})	0.57	0.58	0.67	0.48
		R^2	0.94	0.98	0.97	0.96
D-W	*298*	$K^* \cdot 10^2$	1.92	1.63	2.09	1.50
		R^2	0.81	0.95	0.91	0.87
HSDM	*298*	$Ds^* \cdot 10^{11}$	2.30	2.06	2.43	1.95
		R^2	0.79	0.93	0.89	0.85

$^*\alpha$ - initial adsorption rate; β - desorption constant; K - rate constant of adsorption, D_s - surface diffusion coefficient;

Lower statistical correlation coefficients R^2, obtained using D-W and HSDM models, indicate higher suitability of PSO for description of adsorption kinetic. The empirical PSO equation is a very applicable mathematical model for fitting the kinetic data, *i.e.* rate constant is a function of initial concentration of the adsorbate, giving an overall time-dependent change of concentration without consideration of rate limiting step. Evaluation of the rate controlling step and diffusion coefficients is the most significant for designing the water treatment system. Recognition of the contribution of external and internal mass transfers, with determination of specific contribution of diffusional processes inside a pore, represent crucial results obtained from the kinetic data modeling. The surface and pore diffusion coefficients D_s and D_p, respectively, are key influencing factors to the basic diffusion mechanism inside the adsorbent

pore system. Values of both coefficients depend on the nature of the adsorbent, pore network/structure, synthesis method, and on the nature and size of the adsorbate. According to the results of HSDM kinetic data correlation, it could be assumed that contribution of both effects: intra-particular (main) and surface (minor participation), influences overall kinetic of the adsorbate removal. The HSDM model considers surface diffusion as a main rate-controlling step. HSDM could be used to provide an estimation of intra-particular diffusion, when surface diffusion is the main rate limiting step of an overall process. D-W is usually used for modeling of the adsorption processes into or out of a sphere, based on the Fick's second law of diffusion. It showed low statistical validity and satisfactory matching with PSO results, and could not be used for estimation of this adsorption mechanism.

In general, recognition/description of contribution of both external and internal mass transfer processes are of a high value for understanding kinetic and mechanism of adsorption, relationship between diffusional limitation and textural properties, and operative diffusional processes. In that sense, Weber-Morris model was used for estimation of the contribution of mass transfer processes and evaluation of the rate limiting step of the adsorption process [37,70]. According to the intraparticle diffusion plots, q_t *vs.* $t^{0.5}$, it was evident that the adsorption of Cd^{2+} and Ni^{2+} cations on **A-LMS_5** follows two steps, while adsorption of $CrO_4^{2-}/HCrO_4^-$ and $HAsO_4^{2-}/H_2AsO_4^-$ ions follows a three-step mechanism. The first linear region of W-M plot represents the boundary layer diffusion process [70]. This regime is followed by another linear step which represents the intra particle diffusion through pore network [70]. Correlation line of W-M does not cross the origin, and high values of W-M constant C_1 for both cations and oxyanions removal (**Table 5**) indicate that intra-particle diffusion is not the only rate-limiting step; film (surface) diffusion also played an appropriate role to the control of diffusional

transport [70]. At the initial adsorption stage, the diffusion from bulk phase to the exterior surface takes place at a high rate (diffusional transport inside large pores (0.1 – 1 μm); Fig. 5). Second linear part depends on material porosity and it relates to the diffusion inside meso/micropores [50], while this diffusion regime significantly differs for cations and oxyanions. Larger oxyanions are of lower mobility in the pores of lower diameter and thus adsorption rate (*viz* diffusional rate) slows down with steady attainment of equilibrium.

Table 5 Weber-Morris model for the adsorption of Cd^{2+}, Ni^{2+}, $CrO_4^{2-}/HCrO_4^-$ and $HAsO_4^{2-}/H_2AsO_4^-$ on **A-LMS_5** [$C_{i[Cd^{2+}, Ni^{2+}]}$= 10 mg L^{-1}, pH = 6.5; $C_{i[As(V)and\ Cr(VI)]}$ = 10 mg L^{-1}, pH = 6.0, m/V = 1 g L^{-1}]

Intra-particle diffusion	Constants	Cd^{2+}	Ni^{2+}	$CrO_4^{2-}/HCrO_4^-$	$HAsO_4^{2-}/H_2AsO_4^-$
Weber-Morris (Step 1)	k_{p1}* (mg g^{-1} $min^{-0.5}$)	1.267	0.940	1.261	1.087
	C_1(mg g^{-1})	0.449	0.518	0.810	0.054
	R^2	0.991	0.999	0.991	0.999
Weber-Morris (Step 2)	k_{p2}* (mg g^{-1} $min^{-0.5}$)	0.062	0.220	0.441	0.610
	C_2(mg g^{-1})	7.234	5.127	4.399	3.265
	R^2	0.999	0.983	1	1
Weber-Morris (Step 3)	k_{p3}* (mg g^{-1} $min^{-0.5}$)	-	-	0.074	0.037
	C_3 (mg g^{-1})	-	-	7.027	7.398
	R^2	-	-	0.999	1

* k_p- Weber-Morris intra-particular constant;

Such behavior, interpreted by W-M model, indicate that material porosity, structure of hydration shell, charges and diffusional properties, as well as atomic and ionic radius, all play an appropriate role in diffusional limitations. Smaller atomic radii of Cd^{2+} and Ni^{2+} (149 and 161 pm, respectively) compared to two-to-three fold higher of $CrO_4^{2-}/HCrO_4^-$ and $HAsO_4^{2-}/H_2AsO_4^-$ (358 and 306, respectively) indicate the diffusional limitations due to intra-particular diffusion in the second and especially in the third stage, considering oxyanions. Fast saturation in the first

stage (diffusional transport in large pores) is opposite to slow transport in the third stage, as a result of diffusional transport in the mesopore and micropore network of **A-LMS_5** pore system.

3.8. Overview of adsorption capacities of lignin and lignin-based adsorbents

Adsorption capacities for Cd^{2+} ions on lignin-based sorbents show promising improvements: from 6.7–7.5 mg g^{-1} on lignin from beech and poplar wood modified by alkaline glycerol delignification [71], reaching 48.3 mg g^{-1} (pure lignin) [72] and up to 175.4 mg g^{-1} (kraft lignin from black liquor) [73]. However, the later result was obtained on the elevated temperature (40 ^{0}C) following PSO kinetic model fit. Obtained q_{max} of **A-LMS_5** for Cd^{2+} ions in our research reached 74.84 mg g^{-1} at room temperature, with significantly higher rate constant (k_2 = 1.48×10^{-2} g mg^{-1} min^{-1}; **Table 4**). Maximum adsorption capacities for Cr(VI) ions were obtained with magnetite lignin composite (100.9 mg g^{-1}) [74] with relatively high initial concentration of 150 mg L^{-1}. Furthermore, PSO adsorption rate constant was relatively low, k_2 = 0.32×10^{-2} g mg^{-1} min^{-1}. The chitosan–lignin composite obtained 17.8 mg g^{-1} adsorption capacity [25] with initial concentration of 50 mg L^{-1}, and PSO k_2 = 0.18×10^{-2} g $mg^{-1}min^{-1}$. **A-LMS_5** reached 53.49 mg g^{-1} adsorption capacity for Cr(VI) ions, with a lower initial concentration of 10 mg L^{-1} at room temperature, while obtaining higher PSO rate constant k_2 = 1.74×10^{-2} g mg^{-1} min^{-1} (**Table 4**). On the other hand, rate of Ni^{2+} removal notably varied: on chitin-lignin biosorbent material: from 5.28 mg g^{-1} [26], to significantly higher values for a chitin-lignin hybrid material (70.41 mg g^{-1}) [27] with initial concentration up to 100 mg L^{-1} (PSO type 1, k_2 = 0.86 g mg^{-1} min^{-1}). The q_{max} value of a hybrid material is comparable to the adsorption capacity of **A-LMS_5**, reached for Ni^{2+} ions in our research (49.40 mg g^{-1}) and obtained with lower initial concentration of 10 mg L^{-1} at room temperature (PSO k_2 = 0.97×10^{-2} g mg^{-1} min^{-1}). As for the As(V) ion removal, the highest q_{max} value is obtained for sugarcane bagasse adsorbent (11.9

mg g^{-1}) [75] with 65 mg L^{-1} initial concentration, and for pure lignin q_{max} reached 98.65% [76]. For the **A-LMS_5** adsorbent of our research, we are reporting significantly higher adsorption capacity (51.53 mg g^{-1}) for As(V) ion removal (C_i = 10 mg L^{-1}, T = 25^{0}C), at a high removal rate of PSO k_2 = 0.75×10^{-2} g mg^{-1} min^{-1} (**Table 4**).

Overview of maximum adsorption capacities of lignin and lignin-based adsorbents is provided in the **Table S10.** Comparison of maximum adsorption capacities of heavy metal ions/oxyanions removal of lignin based adsorbents reported in literature with those obtained for **A-LMS_5** indicates excellent adsorption performances of **A-LMS_5**.

4. CONCLUSIONS

Through inverse suspension copolymerization of kraft lignin, with poly(ethylene imine) grafting-agent and epoxy chloropropane cross-linker, sodium lauryl sulfate and 5 wt.% sodium alginate solution, high performance **A-LMS_5** bio-sorbent was successfully prepared. FT-IR and XPS analysis confirmed the structure of synthesized **A-LMS_5**, and provided information on participating groups involved in ion binding. The FESEM analysis revealed a highly porous structure. The maximum adsorption capacity for Cd^{2+} oxyanions reached 74.84 mg g^{-1}, which decreased to 54.20 mg g^{-1} for Cr(VI) oxyanions, 53.12 mg g^{-1} for As(V) and 49.42 mg g^{-1} for Ni^{2+} cations. Results of modeling of kinetic data using the PSO model, indicate fast external mass transfer and prominent effect of intra-particle diffusion to overall mass transport inside the pore network. Relatively high adsorption capacities of **A-LMS_5** adsorbent in a batch system are a result of extraordinary kinetics, as obtained by PSO modeling. Calculated PSO rate constants (k_2, g mg^{-1} min^{-1}): 1.48×10^{-2} for Cd^{2+}, 0.97×10^{-2} for Ni^{2+}, 1.73×10^{-2} for CrO_4^{2-}/$HCrO_4^-$ and 0.75×10^{-2} for $H_2AsO_4^-$/$HAsO_4^{2-}$ are significantly higher than some found in the literature. These findings suggest that, with utilization of bio-waste as a resource, synthesized **A-LMS_5**

biosorbent exhibits high adsorption capacity towards toxic heavy metal ions, thus contributing to efficient wastewater treatment processes.

NOTES

The manuscript was written through contributions of all authors. Declaration of interest: none.

ACKNOWLEDGMENT

This work was supported by the Ministry of Education, Science and Technological Development of the Republic of Serbia [grant numbers OI 172057 and III45019], with the contribution of the COST Action CA17128.

REFERENCES

[1] Y. Kong, L. Wang, Y. Ge, H. Su, Z. Li, Lignin xanthate resin–bentonite clay composite as a highly effective and low-cost adsorbent for the removal of doxycycline hydrochloride antibiotic and mercury ions in water, J. Hazard. Mater. (2019). doi:10.1016/j.jhazmat.2019.01.026.

[2] Z. Li, J. Chen, Y. Ge, Removal of Lead Ion and Oil Droplet from aqueous solution by Lignin-Grafted Carbon Nanotubes, Chem. Eng. J. (2016). doi:10.1016/j.cej.2016.09.126.

[3] A. Herrera-Barros, C. Tejada-Tovar, T. Villabona-Ortiz, A.D. Gonzalez-Delgado, J. Benitez-Monroy, A Comparative Study of Cadmium, Nickel and Chromium Adsorption using Residual Biomass from Elaeisguineensis Modified with Al_2O_3 Nanoparticles, Indian J. Sci. Technol. 11 (2018) 1–7. doi:10.17485/ijst/2018/v11i21/124074.

[4] Z. Li, Y. Ge, Application of Lignin and Its Derivatives in Adsorption of Heavy Metal Ions in Water : A Review Application of Lignin and Its Derivatives in Adsorption of Heavy Metal Ions in Water : A Review, (2018). doi:10.1021/acssuschemeng.8b01345.

[5] D. Dax, M.S. Chávez, C. Xu, S. Willför, R.T. Mendonça, J. Sánchez, Cationic hemicellulose-based hydrogels for arsenic and chromium removal from aqueous solutions, Carbohydr. Polym.

111 (2014) 797–805. doi:10.1016/j.carbpol.2014.05.045.

[6] United States Environmental Protection Agency (US EPA), Water Quality Standards, 2014.

[7] F.L. Mi, S.J. Wu, F.M. Lin, Adsorption of copper(II) ions by a chitosan-oxalate complex biosorbent, Int. J. Biol. Macromol. 72 (2015) 136–144. doi:10.1016/j.ijbiomac.2014.08.006.

[8] Y. Ge, Z. Li, Application of Lignin and Its Derivatives in Adsorption of Heavy Metal Ions in Water: A Review, ACS Sustain. Chem. Eng. 6 (2018). doi:10.1021/acssuschemeng.8b01345.

[9] C. Wang, H. Wang, G. Gu, Ultrasound-assisted xanthation of cellulose from lignocellulosic biomass optimized by response surface methodology for Pb(II) sorption, Carbohydr. Polym. 182 (2018) 21–28. doi:10.1016/j.carbpol.2017.11.004.

[10] A. Duval, M. Lawoko, A review on lignin-based polymeric, micro- and nano-structured materials, React. Funct. Polym. 85 (2014) 78–96. doi:10.1016/j.reactfunctpolym.2014.09.017.

[11] S. Gillet, M. Aguedo, L. Petitjean, A.R.C. Morais, A.M. Da Costa Lopes, R.M. Łukasik, P.T. Anastas, Lignin transformations for high value applications: Towards targeted modifications using green chemistry, Green Chem. 19 (2017) 4200–4233. doi:10.1039/c7gc01479a.

[12] A. Beaucamp, Y. Wang, M. Culebras, M.N. Collins, Carbon fibres from renewable resources: the role of the lignin molecular structure in its blendability with biobased poly(ethylene terephthalate), Green Chem. 21 (2019) 5063–5072. doi:10.1039/c9gc02041a.

[13] M.N. Collins, M. Nechifor, F. Tanasă, M. Zănoagă, A. McLoughlin, M.A. Stróżyk, M. Culebras, C.A. Teacă, Valorization of lignin in polymer and composite systems for advanced engineering applications – A review, Int. J. Biol. Macromol. 131 (2019) 828–849. doi:10.1016/j.ijbiomac.2019.03.069.

[14] M. Culebras, H. Geaney, A. Beaucamp, P. Upadhyaya, E. Dalton, K.M. Ryan, M.N. Collins, Bioderived Carbon Nanofibres from Lignin as High Performance Li-Ion Anode Materials, ChemSusChem. 12 (2019) 4516–4521. doi:10.1002/cssc.201901562.

[15] I. Bykov, Characterization of Natural and Technical Lignins using FTIR Spectroscopy, Master Thesis, Luleå Univ. Technol. (2008).

[16] K. Taleb, J. Markovski, Z. Veličković, J. Rusmirović, M. Rančić, V. Pavlovic, A. Marinković, Arsenic removal by magnetite-loaded amino modified nano/microcellulose adsorbents: Effect of functionalization and media size, Arab. J. Chem. Article (2016). doi:10.1016/j.arabjc.2016.08.006.

[17] Y. Wang, X. Cao, S. Sun, R. Zhang, Q. Shi, L. Zheng, R. Sun, Carbon microspheres prepared from the hemicelluloses-rich pre-hydrolysis liquor for contaminant removal, Carbohydr. Polym. 213 (2019) 296–303. doi:10.1016/j.carbpol.2019.02.029.

[18] Y. Li, M. Wu, B. Wang, Y. Wu, M. Ma, X. Zhang, Synthesis of Magnetic Lignin-Based Hollow Microspheres: A Highly Adsorptive and Reusable Adsorbent Derived from Renewable Resources, ACS Sustain. Chem. Eng. 4 (2016) 5523–5532. doi:10.1021/acssuschemeng.6b01244.

[19] Z. Li, D. Xiao, Y. Kong, Y. Ge, Enhancing lead adsorption capacity by controlling the chain length of alkyl amine grafted lignin, BioResources. 10 (2015) 2425–2432. doi:10.15376/biores.10.2.2425-2432.

[20] B. Podkościelna, M. Goliszek, O. Sevastyanova, New approach in the application of lignin for the synthesis of hybrid materials, Pure Appl. Chem. 89 (2017) 161–171. doi:10.1515/pac-2016-1009.

[21] F.B. Liang, Y.L. Song, C.P. Huang, Y.X. Li, B.H. Chen, Synthesis of novel lignin-based ion-exchange resin and its utilization in heavy metals removal, Ind. Eng. Chem. Res. 52 (2013) 1267–1274. doi:10.1021/ie301863e.

[22] L. Dai, Y. Li, R. Liu, C. Si, Y. Ni, Green mussel-inspired lignin magnetic nanoparticles with high adsorptive capacity and environmental friendliness for chromium(III) removal, Int. J. Biol. Macromol. 132 (2019) 478–486. doi:10.1016/j.ijbiomac.2019.03.222.

[23] Z. Li, J. Chen, Y. Ge, Removal of lead ion and oil droplet from aqueous solution by lignin-grafted carbon nanotubes, Chem. Eng. J. 308 (2017) 809–817. doi:10.1016/j.cej.2016.09.126.

[24] D. Xiao, W. Ding, J. Zhang, Y. Ge, Z. Wu, Z. Li, Fabrication of a versatile lignin-based nano-trap for heavy metal ion capture and bacterial inhibition, Chem. Eng. J. 358 (2019) 310–320. doi:10.1016/j.cej.2018.10.037.

[25] V. Nair, A. Panigrahy, R. Vinu, Development of novel chitosan-lignin composites for adsorption

of dyes and metal ions from wastewater, Chem. Eng. J. 254 (2014) 491–502. doi:10.1016/j.cej.2014.05.045.

[26] M. Wysokowski, Ł. Klapiszewski, D. Moszyński, P. Bartczak, T. Szatkowski, I. Majchrzak, K. Siwińska-Stefańska, V. V. Bazhenov, T. Jesionowski, Modification of chitin with kraft lignin and development of new biosorbents for removal of cadmium(II) and nickel(II) ions, Mar. Drugs. 12 (2014) 2245–2268. doi:10.3390/md12042245.

[27] P. et al. Bartczak, Treatment of model solutions and wastewater containing selected hazardous metal ions using a chitin/lignin hybrid material, J. Environ. Manage. (2017) 300–310. doi:.1037//0033-2909.I26.1.78.

[28] E. Larrañeta, M. Imízcoz, J.X. Toh, N.J. Irwin, A. Ripolin, A. Perminova, J. Domínguez-Robles, A. Rodríguez, R.F. Donnelly, Synthesis and Characterization of Lignin Hydrogels for Potential Applications as Drug Eluting Antimicrobial Coatings for Medical Materials, ACS Sustain. Chem. Eng. 6 (2018) 9037–9046. doi:10.1021/acssuschemeng.8b01371.

[29] J. Li, H. Li, Z. Yuan, J. Fang, L. Chang, H. Zhang, C. Li, Role of sulfonation in lignin-based material for adsorption removal of cationic dyes, Int. J. Biol. Macromol. 135 (2019) 1171–1181. doi:10.1016/j.ijbiomac.2019.06.024.

[30] M. Ahmad, B. Zhang, J. Wang, J. Xu, K. Manzoor, S. Ahmad, S. Ikram, New method for hydrogel synthesis from diphenylcarbazide chitosan for selective copper removal, Int. J. Biol. Macromol. 136 (2019) 189–198. doi:10.1016/j.ijbiomac.2019.06.084.

[31] A. Popovic, J. Rusmirovic, S. Levic, A. Bozic, T. Kovacevic, Amino-functionalized lignin microsperes: Synthesis and characterization of high-performance adsorbent for effective nickel(II) ion removal, in: 31st Int. Congr. Prcess Ind., 2018: pp. 235–239.

[32] B. Yu, Z. Chang, Y. Zhang, C. Wang, Preparation and formation mechanism of size-controlled lignin based microsphere by reverse phase polymerization, Mater. Chem. Phys. 203 (2018) 97–105. doi:10.1016/j.matchemphys.2017.08.039.

[33] J. Sameni, S. Krigstin, S.A. Jaffer, M. Sain, Preparation and characterization of biobased

microspheres from lignin sources, Ind. Crops Prod. 117 (2018) 58–65. doi:10.1016/j.indcrop.2018.02.078.

[34] B. Podkościelna, O. Gordobil, A. V. Riazanova, G. Dobele, J. Labidi, M.E. Lindström, V.M. Gun'ko, O. Sevastyanova, Novel Porous Materials Obtained from Technical Lignins and Their Methacrylate Derivatives Copolymerized with Styrene and Divinylbenzene, ChemistrySelect. 2 (2017) 2257–2264. doi:10.1002/slct.201601827.

[35] Y. Ge, L. Qin, Z. Li, Lignin microspheres: An effective and recyclable natural polymer-based adsorbent for lead ion removal, Mater. Des. 95 (2016) 141–147. doi:10.1016/j.matdes.2016.01.102.

[36] H. Sontheimer, J.C. Crittenden, S. R. Scott, Activated carbon for water treatment, in: Act. Carbon Water Treat., Second, DVGW-Forschungsstelle, Engler-Bunte-Institut, Universitat Karlsruhe, 1988: pp. 66–67.

[37] G.D. Vuković, A.D. Marinković, S.D. Škapin, M.T. Ristić, R. Aleksić, A. a. Perić-Grujić, P.S. Uskoković, Removal of lead from water by amino modified multi-walled carbon nanotubes, Chem. Eng. J. 173 (2011) 855–865. doi:10.1016/j.cej.2011.08.036.

[38] H. Xiyili, S. Çetintaş, D. Bingöl, Removal of some heavy metals onto mechanically activated fly ash: Modeling approach for optimization, isotherms, kinetics and thermodynamics, Process Saf. Environ. Prot. 109 (2017) 288–300. doi:10.1016/j.psep.2017.04.012.

[39] R.J.A. Gosselink, Lignin as a renewable aromatic resource for the chemical industry, 2011. doi:ISBN: 978-94-6173-100-5.

[40] Y. Ge, Z. Li, D. Xiao, P. Xiong, N. Ye, Sulfonated multi-walled carbon nanotubes for the removal of copper (II) from aqueous solutions, J. Ind. Eng. Chem. 20 (2014) 1765–1771. doi:10.1016/j.jiec.2013.08.030.

[41] J. Chen, W. Liu, Z. Song, H. Wang, Y. Xie, Photocatalytic Degradation of β-O-4 Lignin Model Compound by In2S3 Nanoparticles Under Visible Light Irradiation, Bioenergy Res. 11 (2017) 166–173. doi:10.1007/s12155-017-9886-8.

[42] S.V. Harb, B.M. Cerrutti, S.H. Pulcinelli, C.V. Santilli, P. Hammer, Siloxane-PMMA hybrid anti-corrosion coatings reinforced by lignin, Surf. Coatings Technol. 275 (2015) 9–16. doi:10.1016/j.surfcoat.2015.05.002.

[43] C. Te Hsieh, D.Y. Tzou, K.Y. Hsieh, K.M. Yin, Photoluminescence from amino functionalized graphene quantum dots prepared by electrochemical exfoliation method in the presence of ammonium ions, RSC Adv. 7 (2017) 18340–18346. doi:10.1039/c6ra28742e.

[44] C. Zhang, R. Hao, H. Liao, Y. Hou, Synthesis of amino-functionalized graphene as metal-free catalyst and exploration of the roles of various nitrogen states in oxygen reduction reaction, Nano Energy. 2 (2013) 88–97. doi:10.1016/j.nanoen.2012.07.021.

[45] H. Gao, S. Yan, J. Wang, Y.A. Huang, P. Wang, Z. Li, Z. Zou, Towards efficient solar hydrogen production by intercalated carbon nitride photocatalyst, Phys. Chem. Chem. Phys. 15 (2013) 18077. doi:10.1039/c3cp53774a.

[46] C. Wang, T. Liu, Nori-based N, O, S, Cl co-doped carbon materials by chemical activation of ZnCl2 for supercapacitor, J. Alloys Compd. 696 (2017) 42–50. doi:10.1016/j.jallcom.2016.11.206.

[47] L. Štrbková, A. Manakhov, L. Zajíčková, A. Stoica, P. Veselý, R. Chmelík, The adhesion of normal human dermal fibroblasts to the cyclopropylamine plasma polymers studied by holographic microscopy, Surf. Coatings Technol. 295 (2016) 70–77. doi:10.1016/j.surfcoat.2015.10.076.

[48] A. Sood, Particle size distribution control in emulsion polymerization, J. Appl. Polym. Sci. 92 (2003) 2884–2902.

[49] I. Capek, Inverse Emulsion Polymerization of Acrylamide Initiated by Oil- and Water-soluble Initiators : Effect of Emulsifier Concentration, 36 (2004) 793–803. doi:10.1295/polymj.36.793.

[50] J.D. Rusmirović, N. Obradović, J. Perendija, A. Umićević, A. Kapidžić, B. Vlahović, V. Pavlović, A.D. Marinković, V.B. Pavlović, Controllable synthesis of Fe3O4-wollastonite adsorbents for efficient heavy metal ions/oxyanions removal, Environ. Sci. Pollut. Res. (2019). doi:10.1007/s11356-019-04625-0.

[51] M.A. Ahmed, S.M. Ali, S.I. El-Dek, A. Galal, Magnetite–hematite nanoparticles prepared by green methods for heavy metal ions removal from water, Mater. Sci. Eng. B. 178 (2013) 744–751. doi:10.1016/j.mseb.2013.03.011.

[52] S. Rajput, C.U. Pittman, D. Mohan, Magnetic magnetite (Fe3O4) nanoparticle synthesis and applications for lead (Pb 2+) and chromium (Cr 6+) removal from water, J. Colloid Interface Sci. 468 (2016) 334–346. doi:10.1016/j.jcis.2015.12.008.

[53] J.P. Gustafsson, Visual MINTEQ. 3.0, beta, (2011).

[54] A. Drah, N.Z. Tomić, Z. Veličić, A.D. Marinković, Ž. Radovanović, Z. Veličković, R. Jančić-Heinemann, Highly ordered macroporous γ -alumina prepared by a modified sol-gel method with a PMMA microsphere template for enhanced Pb 2+ , Ni 2+ and Cd 2+ removal, Ceram. Int. 43 (2017) 13817–13827. doi:10.1016/j.ceramint.2017.07.102.

[55] O. Takabasbi, K. Saito, A theoretical study of cadmium-ethylenediamine and -ammonia exciplexes. Comparison with experiments, 207 (1993) 379–383.

[56] W. Zhan, L. Gao, X. Fu, S. Hussain, G. Sui, X. Yang, Green synthesis of amino-functionalized carbon nanotube-graphene hybrid aerogels for high performance heavy metal ions removal, Appl. Surf. Sci. 467–468 (2019) 1122–1133. doi:10.1016/j.apsusc.2018.10.248.

[57] M. Kumari, C.U. Pittman, D. Mohan, Heavy metals [chromium (VI) and lead (II)] removal from water using mesoporous magnetite (Fe_3O_4) nanospheres, J. Colloid Interface Sci. 442 (2015) 120–132. doi:10.1016/j.jcis.2014.09.012.

[58] L. Niu, S. Deng, G. Yu, J. Huang, Efficient removal of Cu (II), Pb (II), Cr (VI) and As (V) from aqueous solution using an aminated resin prepared by surface-initiated atom transfer radical polymerization, Chem. Eng. J. 165 (2010) 751–757. doi:10.1016/j.cej.2010.08.053.

[59] F. Rouquerol, J. Rouquerol, Sing, Kenneth, Adsorption by powders and porous solids: Principles, methodology and application, Academic Press, USA, 1999.

[60] K.Y. Foo, B.H. Hameed, Insights into the modeling of adsorption isotherm systems, Chem. Eng. J. 156 (2010) 2–10. doi:10.1016/j.cej.2009.09.013.

[61] Z. Veličković, G.D. Vuković, A.D. Marinković, M.S. Moldovan, A.A. Perić-Grujić, P.S. Uskoković, M.D. Ristić, Adsorption of arsenate on iron(III) oxide coated ethylenediamine functionalized multiwall carbon nanotubes, Chem. Eng. J. 181–182 (2012) 174–181. doi:10.1016/j.cej.2011.11.052.

[62] D. Budimirović, Z.S. Veličković, V.R. Djokić, M. Milosavljević, J. Markovski, S. Lević, A.D. Marinković, Efficient As(V) removal by α -FeOOH and α-FeOOH/ α-MnO2 embedded PEG-6-arm functionalized multiwall carbon nanotubes, Chem. Eng. Res. Des. 119 (2017) 75–86. doi:10.1016/j.cherd.2017.01.010.

[63] C.-H. Liu, Y.-H. Chuang, T.-Y. Chen, Y. Tian, H. Li, M.-K. Wang, W. Zhang, Mechanism of Arsenic Adsorption on Magnetite Nanoparticles from Water: Thermodynamic and Spectroscopic Studies, Environ. Sci. Technol. 49 (2015) 7726–7734. doi:10.1021/acs.est.5b00381.

[64] L. Sellaoui, G.L. Dotto, A. Ben Lamine, A. Erto, Interpretation of single and competitive adsorption of cadmium and zinc on activated carbon using monolayer and exclusive extended monolayer models, Environ. Sci. Pollut. Res. 24 (2017) 19902–19908. doi:10.1007/s11356-017-9562-8.

[65] L. Sellaoui, F. Edi Soetaredjo, S. Ismadji, É.C. Lima, G.L. Dotto, A. Ben Lamine, A. Erto, New insights into single-compound and binary adsorption of copper and lead ions on treated sea mango shell: Experimental and theoretical studies, Phys. Chem. Chem. Phys. 19 (2017) 25927–25937. doi:10.1039/c7cp03770h.

[66] Y. Ge, X. Cui, C. Liao, Z. Li, Facile fabrication of green geopolymer/alginate hybrid spheres for efficient removal of Cu(II) in water: Batch and column studies, Chem. Eng. J. 311 (2017) 126–134. doi:10.1016/j.cej.2016.11.079.

[67] O. Bizerea Spiridon, L. Pitulice, Response to "Using of 'pseudo-second-order model' in adsorption", comment letter on "Phenol removal from wastewater by adsorption on zeolitic composite" [Bizerea Spiridon et al., Environ Sci Pollut Res (2013) 20:6367–6381], Environ. Sci. Pollut. Res. 21 (2014) 7236–7237. doi:10.1007/s11356-014-2705-2.

[68] H. Qiu, L. Lv, B. Pan, Q.Q. Zhang, W. Zhang, Q.Q. Zhang, Critical review in adsorption kinetic models, J. Zhejiang Univ. Sci. A. 10 (2009) 716–724. doi:10.1631/jzus.A0820524.

[69] M.M. Haring, The Theory of Rate Processes (Glasstone, Samuel; Laidler, Keith J.; Eyring, Henry), J. Chem. Educ. 19 (1942) 249. doi:10.1021/ed019p249.1.

[70] S. Nethaji, A. Sivasamy, A.B. Mandal, Adsorption isotherms, kinetics and mechanism for the adsorption of cationic and anionic dyes onto carbonaceous particles prepared from Juglans regia shell biomass, Int. J. Environ. Sci. Technol. 10 (2013) 231–242. doi:10.1007/s13762-012-0112-0.

[71] A. Demirbas, Adsorption of Co(II) and Hg(II) from water and wastewater onto modified lignin, Energy Sources, Part A Recover. Util. Environ. Eff. 29 (2007) 117–123. doi:10.1080/009083190948720.

[72] M.C. Basso, E.G. Cerrella, A.L. Cukierman, Cadmium Uptake by Lignocellulosic Materials: Effect of Lignin Content, Sep. Sci. Technol. 39 (2004) 1163–1175. doi:10.1081/ss-120028577.

[73] D. Mohan, C.U. Pittman, P.H. Steele, Single, binary and multi-component adsorption of copper and cadmium from aqueous solutions on Kraft lignin-a biosorbent, J. Colloid Interface Sci. 297 (2006) 489–504. doi:10.1016/j.jcis.2005.11.023.

[74] Z. Song, W. Li, W. Liu, Y. Yang, N. Wang, H. Wang, H. Gao, Novel magnetic lignin composite sorbent for chromium(<scp>vi</scp>) adsorption, RSC Adv. 5 (2015) 13028–13035. doi:10.1039/C4RA15546G.

[75] H. Tajernia, T. Ebadi, B. Nasernejad, M. Ghafori, Arsenic removal from water by sugarcane bagasse: An application of response surface methodology (RSM), Water. Air. Soil Pollut. 225 (2014). doi:10.1007/s11270-014-2028-4.

[76] Y.F. Xu, X. Wan, X.K. OuYang, Q. Di Yu, L.Y. Yang, W. La Li, Removal of Arsenic Ion from Aquatic Condiment Using Lignin, Adv. Mater. Res. 554–556 (2012) 2080–2084. doi:10.4028/www.scientific.net/amr.554-556.2080.

Graphical Abstract

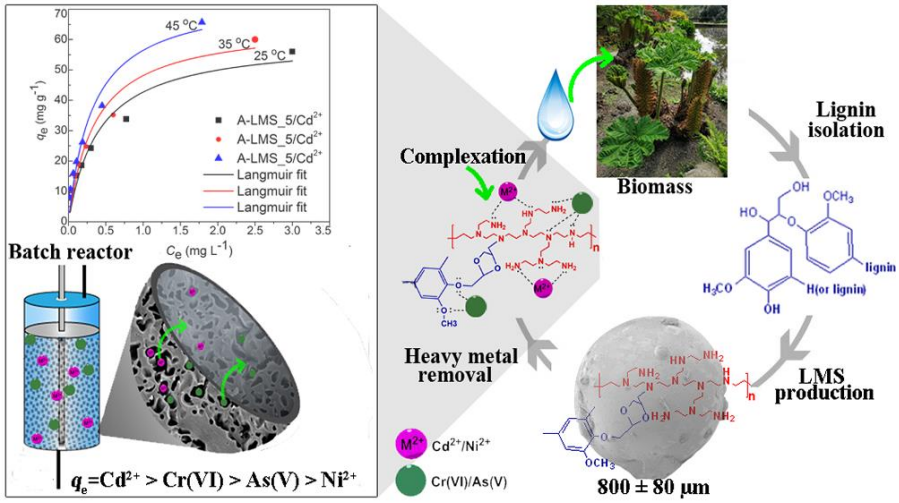

List of Figures

Fig. 1 Possible a) mechanism of the A_LMS microsphere formation; and b) formation of complexes with Ni^{2+}, Cd^{2+}, Cr(VI), and As(V)

Fig. 2 3D (a) and 2D (b) plots of dependence of the amino groups content *versus* lignin content and alginate concentration

Fig. 3 FT-IR and XPS spectra of lignin and synthesized **A-LMS_1**, **A-LMS_5** and **A-LMS_10**: a) FTIR, b) Survey, c) C1 s, d) O 1s, e) Cl 2p, f) N 1s (Label Δin Fig. 3d stands for the difference: $BE(2p_{1/2})$-$BE(2p_{3/2})$)

Fig. 4 FESEM micrographs of A-LMS_1 (a, b, c), A-LMS_5 (d, e, f) and A-LMS_10 (g, h, i)

Fig. 5 Influence of pH on Cd^{2+}, Ni^{2+}, $HAsO_4^{2-}/H_2AsO_4^-$ and $CrO_4^{2-}/HCrO_4^-$ ions removal by **A-LMS_5** (C_i = 1 g L^{-1}, m/V = 1 g L^{-1}, T = 308 K)

Fig. 6 FTIR spectrum of **A-LMS_5** after adsorption

CRediT author statement

Ana L. Popovic: Conceptualization, Investigation, Data curation, Writing - original draft preparation;
Jelena D. Rusmirovic: Methodology, Visualization, Writing - reviewing and editing;
Zlate Velickovic: Software, Investigation, Data Curation;
Zeljko Radovanovic: Investigation, Software;
Mirjana Ristic: Data Curation, Writing - reviewing and editing;
Vera P. Pavlovic: Investigation;
Aleksandar D. Marinkovic: Resources, Validation, Supervision.

Highlights

- Synthesis of amino-functionalized lignin microspheres (A-LMS) was optimized
- Boosted adsorption efficiency of Ni^{2+}, Cd^{2+}, As(V) and Cr(VI) ions on A-LMS
- Modeling of adsorption, kinetic and thermodynamic data investigated
- Pseudo-second order kinetic model indicates very fast removal rates